Geochemistry, Geophysics, Geosystems

RESEARCH ARTICLE
10.1029/2018GC007810

Imaging Slab Detachment Within the Western Hellenic Subduction Zone

Samantha E. Hansen[1], **Christos P. Evangelidis**[2], **and Gerassimos A. Papadopoulos**[2]

[1]Geological Sciences Department, The University of Alabama, Tuscaloosa, AL, USA, [2]Institute of Geodynamics, National Observatory of Athens, Athens, Greece

Key Points:
- New tomographic model highlights slab structure between ~150- and 250-km depth in the Western Hellenic Subduction Zone
- Trench-parallel tear extends between northern Greece and the Gulf of Corinth; slab thinned but not detached beneath Peloponnese
- Interpreted tear geometry correlates with seismicity and volcanic centers

Supporting Information:
- Supporting Information S1

Correspondence to:
S. E. Hansen,
shansen@geo.ua.edu

Citation:
Hansen, S. E., Evangelidis, C. P., & Papadopoulos, G. A. (2019). Imaging slab detachment within the Western Hellenic Subduction Zone. *Geochemistry, Geophysics, Geosystems*, *20*. https://doi.org/10.1029/2018GC007810

Received 3 JUL 2018
Accepted 16 JAN 2019
Accepted article online 20 JAN 2019

Abstract The Western Hellenic Subduction Zone (WHSZ) has been the focus of numerous seismic investigations, but its structure, particularly between ~150- and 250-km depth, remains poorly understood. Many questions exist regarding the slab geometry at these intermediate depths, including whether the slab displays any tears related to tectonic processes along the WHSZ; however, local and regional studies only provide limited depth coverage, and the coarser resolution associated with broader-scale investigations makes it difficult to discern detailed slab structure. Here, we have employed an adaptively parameterized inversion scheme to develop a new *P* wave tomography model for the WHSZ that bridges the gap between regional- and broader-scale studies. Our new model highlights a trench-parallel tear in the subducting lithosphere between northern Greece and the Gulf of Corinth. Further south, the imaged velocity structure indicates that the slab is retreating to the west and that it is thinned by the southward propagating tear, but the slab has not yet detached in this area. The tear well correlates with the down-dip limit of seismicity in central Greece, while the steeply dipping slab between ~60- and 200-km depth beneath southern Greece coincides with a steeper and deeper Wadati-Benioff zone. While the slab continues into the lower mantle, earthquakes terminate at ~200-km depth, and this is best attributed to dehydration processes in the subducting lithosphere. The southern extent of the tear imaged in our study also coincides with volcanic centers in eastern Peloponnese. Our results suggest that the trench-parallel tear strongly influences seismicity and volcanism throughout Greece.

Plain Language Summary Along the Western Hellenic Subduction Zone (WHSZ), continental material is descending beneath northern Greece, while oceanic material is descending beneath southern Greece. Whether this material displays any gaps or tears at depth is a question of significant debate. Using imaging techniques based on earthquake data recorded by seismic stations throughout Greece, our study highlights the structure within the WHSZ. Our findings illustrate that the subducted material is torn between ~150- and 250-km depth north of the Gulf of Corinth. Further south, the subducting material is thinned by the tear, but it has not completely detached. The interpreted structure well correlates with previously identified patterns of seismicity throughout Greece as well as the locations of volcanoes.

1. Introduction

The Western Hellenic Subduction Zone (WHSZ; Figure 1) has long been recognized as a complicated tectonic environment, associated with variable convergence rates, different lithospheric compositions, and abundant seismicity. Given this, it has been the focus of numerous geological and geophysical investigations (see section 2); however, connecting surface observations to the structure at depth remains a challenge. In particular, the geometry of the subducting slab beneath the WHSZ is still poorly understood. Local and regional seismic investigations (e.g., Halpaap et al., 2018; Papazachos & Nolet, 1997; Pearce et al., 2012; Sodoudi et al., 2015; Tiberi et al., 2000) have yielded important information about the shallow WHSZ structure, but these studies typically only provide constraints down to ~150-km depth. Deeper structure is constrained by broader-scale models (e.g., Hosa, 2008; Koulakov et al., 2009; Piromallo & Morelli, 2003; Spakman et al., 1988; Zhu et al., 2015) but with coarser resolution (usually ~150–500 km). The slab structure between ~150- and 250-km depth remains a topic of significant debate, particularly whether the slab displays any trench-parallel and/or trench-perpendicular tears associated with regional tectonic processes. This portion of the subduction zone is also associated with the termination of seismicity within the WHSZ (e.g., Bocchini et al., 2018; Halpaap et al., 2018) and likely influences volcanism within the Hellenic arc (e.g., Pe-Piper & Piper, 2007).

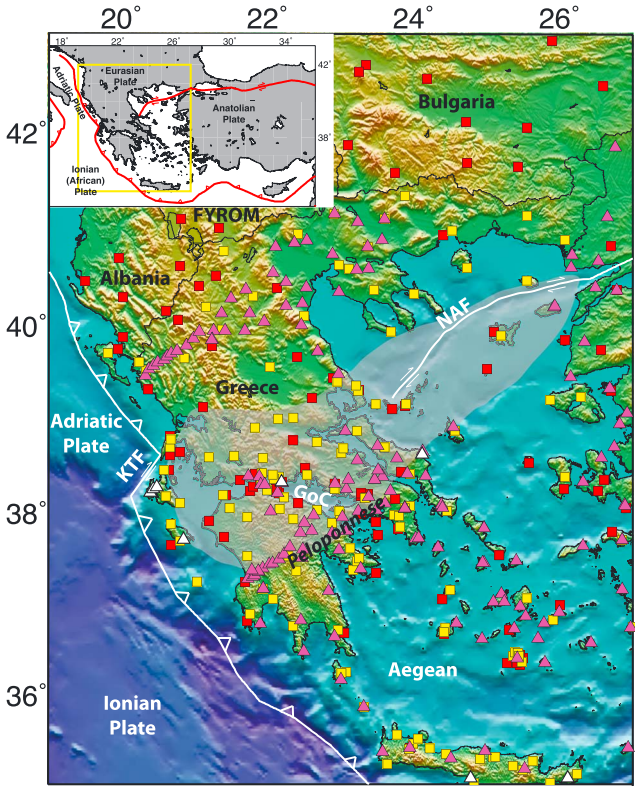

Figure 1. Map of the study area and associated seismic stations. Inset shows the broader Mediterranean area with plate boundaries from Bird (2003) marked in red. The yellow box denotes the study area in the main map. On the main map, white lines mark plate boundaries, and the gray-shaded area denotes the central Hellenic shear zone, as defined by Royden and Papanikolaou (2011). Red squares denote stations that are part of the global ISC catalog only. Yellow squares highlight HUSN stations that are included in the ISC catalog, and additional data have been added for these stations. Triangles denote augmented stations, where white triangles denote HUSN stations and purple triangles denote other deployments. NAF: North Anatolian Fault; KTF: Kefalonia Transform Fault; GoC: Gulf of Corinth; FYROM: Former Yugoslav Republic of Macedonia.

In this study, we have used travel-times from regional and teleseismic events recorded by stations throughout Greece, in conjunction with those from the global International Seismological Centre (ISC) catalog, to generate a new *P* wave tomography model for the WHSZ. Our model has been constructed with an adaptively parameterized grid based on the data-sampling density, and the combined data set and methodology allow us to bridge the resolution gap between regional-scale and broader, Mediterranean- or global-scale tomographic investigations. The major contribution of our new model is the high-resolution imaging of subducting slab structure between ~150- and 250-km depth, which allows us to address many questions regarding the WHSZ geometry and its relation to seismicity and volcanism.

2. Geodynamic Setting and Previous Studies

The Hellenic arc stretches over 1,000 km, from the southeastern Adriatic Sea in the north to the southern Mediterranean, and it marks a convergent boundary where the African plate is subducting beneath the Eurasian and Anatolian plates (Figure 1). The western portion of the system extends ~400 km along the western coast of Greece, where convergence has been associated with the subduction of multiple ocean basins, interspersed with continental units, between the Jurassic-Cretaceous and the present day (e.g., Dercourt et al., 1986; Ricou et al., 1998; Robertson et al., 1996; van Hinsbergen et al., 2005). Current GPS studies (e.g., Hollenstein et al., 2008; McClusky et al., 2000; Reilinger et al., 2010) show that the rate of subduction is variable along the WHSZ, averaging ~8 mm/year beneath northern Greece and ~40 mm/year beneath southern Greece. This variability is attributed to a number of factors. Both marine and terrestrial seismic investigations (e.g., de Voogd et al., 1992; Finetti et al., 1991; Finetti & Del Ben, 2005; Kokinou et al., 2005; Pearce et al., 2012) have shown that less dense, continental lithosphere associated with the Adriatic microplate is being subducted north of ~38°N latitude, while more dense oceanic lithosphere in the Ionian Sea is being subducted further to the south (Figure 1). The positively buoyant continental lithosphere likely resists subduction beneath northern Greece (Taymaz et al., 1991), leading to reduced convergence rates in this area. Additionally, collisional forces further to the east drive the Aegean region southward, causing it to actively override the subducting lithosphere, thereby leading to rapid convergence along the southern portion of the WHSZ (McClusky et al., 2000). Sinking forces associated with the subducting oceanic plate (i.e., slab rollback) may also contribute to the large relative displacement in southern Greece (Bohnhoff et al., 2005; McClusky et al., 2000; Sachpazi et al., 2016).

The Adriatic continental microplate is laterally offset by ~100–140 km from the Ionian oceanic plate along the Kefalonia Transform Fault (KTF; Figure 1), which helps to accommodate the differential rollback between the two segments (Hollenstein et al., 2008; Kahle & Mueller, 1998; Royden & Papanikolaou, 2011). Dextral motion along the KTF may be connected to that along the North Anatolian Fault (NAF) across the ~100-km-wide Central Hellenic Shear Zone (CHSZ; Figure 1), which includes an area of rapid extension in the Gulf of Corinth (Nixon et al., 2016; Papanikolaou & Royden, 2007; Royden & Papanikolaou, 2011). However, the CHSZ is dominated by E-W and NW-SE striking normal faults (Bell et al., 2009), and it has been suggested that the strain field in this area is not associated with dextral shear motion (Pérouse et al., 2012). Moreover, Chousianitis et al. (2015) detected two pairs of shear belts, one in western Greece and northwestern Peloponnese and one in the North Aegean, but they found no evidence for NAF extension toward central Greece. Therefore, it is unclear from surface observations how the boundary between the continental and oceanic lithosphere affects structure at depth.

Given this, the WHSZ has been the focus of numerous seismic investigations, with local and regional studies providing important constraints on the shallow structure, typically down to ~150-km depth. Offshore, active-source reflection and refraction profiles have imaged thin (<7 km) oceanic crust entering the trench south of the KTF (e.g., Bohnhoff et al., 2001; Kokinou et al., 2005, 2006). However, to the north, 19- to 30-km thick continental crust is imaged within the Adriatic (Del Ben et al., 2015; Finetti & Del Ben, 2005). The interplate boundary has been imaged in the vicinity of the Ionian islands (Clément et al., 2000). Moving inland, receiver function (Endrun et al., 2005; Gesret et al., 2011; Li et al., 2003; Sachpazi et al., 2016; Sodoudi et al., 2015) and scattered waves analyses (Pearce et al., 2012; Suckale et al., 2009) have imaged the crust of the subducting lithosphere between ~35- and 100-km depth. The oceanic Ionian slab appears to be segmented by along-dip faults (Sachpazi et al., 2016), and while detailed estimates of the plate thickness are not available (Bocchini et al., 2018), previous studies estimate a plate thickness of 100–150 km, consistent with old oceanic lithosphere (Bijwaard et al., 1998; Bocchini et al., 2018; Koulakov et al., 2009; Piromallo & Morelli, 2003; Spakman et al., 1988; Zhu et al., 2015). Local and regional travel-time tomography (Halpaap et al., 2018; Lamara, 2014; Ligdas et al., 1990; Papazachos & Nolet, 1997; Tiberi et al., 2000) has also been employed to assess the slab structure at these depths. Generally, the subducting lithosphere is imaged as a seismically fast anomaly down to ~150-km depth; however, it has been suggested that the subduction dip angle abruptly changes between ~70- and 90-km depth. At shallow depths, the subducting slab has a gentle ~10–25° dip; however, the dip then increases to 45° or even 60° (Halpaap et al., 2018; Papazachos & Nolet, 1997; Pearce et al., 2012; Sodoudi et al., 2015; Tiberi et al., 2000).

Shallow seismic imaging constraints are complimented by earthquake relocation studies and investigations of seismicity patterns within the WHSZ (Bocchini et al., 2018; Brüstle, 2012; Durand et al., 2014; Galanis et al., 2006; Halpaap et al., 2018; Karakonstantis & Papadimitriou, 2010; Karastathis et al., 2015; Papazachos et al., 2000). While earthquakes above ~40-km depth are prevalent throughout Greece, intermediate-depth seismicity associated with the subducting slab is sparse north of the KTF. Two recent studies by Halpaap et al. (2018) and Bocchini et al. (2018) show an abrupt change in seismicity just south of the KTF, where intermediate-depth earthquakes occur down to ~70- to 100-km depth. South of the Gulf of Corinth (Figure 1), earthquakes occur down to ~190-km depth and define a steeper Wadati-Benioff zone (Bocchini et al., 2018; Halpaap et al., 2018; Papazachos et al., 2000), comparable to the increased dip angle suggested by seismic imaging in this region (Papazachos & Nolet, 1997; Pearce et al., 2012; Sodoudi et al., 2015; Tiberi et al., 2000). Sachpazi et al. (2016) suggested that the intermediate-depth events cluster along dip-parallel faults that segment the oceanic slab. No earthquakes deeper than ~200 km have been observed in the WHSZ.

The deep structure of the WHSZ has been largely constrained by broader, Mediterranean- and global-scale tomographic studies, based on both surface and body wave constraints (Bijwaard et al., 1998; Bourova et al., 2005; Di Luccio & Pasyanos, 2007; Endrun et al., 2008; Hosa, 2008; Konstantinou & Melis, 2008; Koulakov et al., 2009; Li et al., 2008; Pasyanos & Walter, 2002; Piromallo & Morelli, 2003; Salaün et al., 2012; Schmid et al., 2006; Spakman et al., 1988, 1993; Zhu et al., 2015). These studies generally show a seismically fast anomaly trending to the northeast beneath the WHSZ, extending well into the lower mantle (down to ~1,400 km), and this feature has been interpreted as subducted slab at depth. However, while continuous slab across the transition zone is widely accepted, the structure in the upper mantle, particularly between ~150- and 250-km depth, is debated. This is largely due to the limited depth constraints provided by local and regional studies and the coarser resolution associated with broader-scale imaging. Indeed, in some cases, the presence of the slab at these upper mantle depths is only inferred from seismicity as it is not imaged by tomography (e.g., Hosa, 2008; Li et al., 2008; Spakman et al., 1988).

Of particular interest are whether there are any tears or detachments in the subducting slab beneath the WHSZ. For instance, some studies (e.g., Hosa, 2008; Koulakov et al., 2009; Pearce et al., 2012; Spakman et al., 1988, 1993; Zhu et al., 2015) show discontinuous or faded slab structure in the upper mantle, and this has been interpreted to potentially reflect a trench-parallel tear, propagating from north to south (e.g., Carminati et al., 1998; Wortel & Spakman, 1992, 2000; Figure 2a). The depth at which this tear may occur varies between ~150 and 500 km, depending on the model, and there are also discrepancies over the southernmost extent of the tear. For instance, Zhu et al. (2015) suggest that the tear only affects northern Greece, but Spakman et al. (1988) and Meijer and Wortel (1996) suggest that the tear continues into southern Peloponnese. In contrast, other studies (e.g., Konstantinou & Melis, 2008; Piromallo & Morelli, 2003;

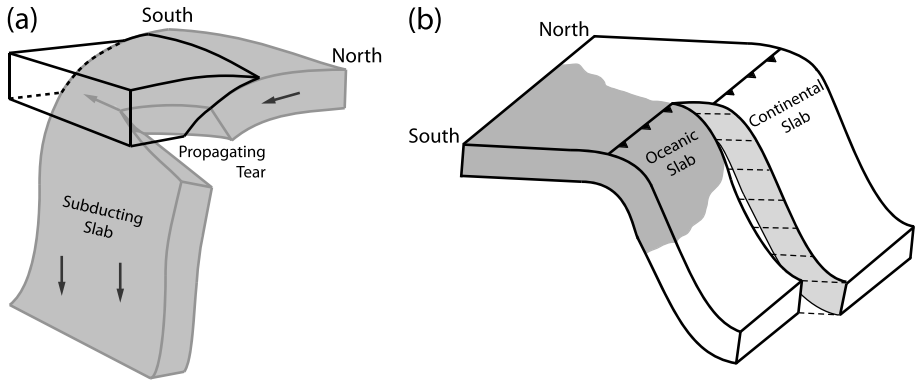

Figure 2. Cartoons illustrating possible slab structure. (a) Proposed horizontal tear in the subducting lithosphere, propagating from north to south. Modified from Wortel and Spakman (2000). (b) Possible structure between the northern, continental and southern, oceanic segments of the subducting slab. The area marked with dashed lines may be torn or warped into a ramp-like structure. Modified from Pearce et al. (2012).

Sodoudi et al., 2006) do not advocate for a trench-parallel tear and instead suggest continuous structure at these depths. Further, a trench-perpendicular tear has also been suggested, potentially marking the continuation of the KTF and accommodating the differential motion between the subducting continental and oceanic lithosphere beneath northern and southern Greece, respectively (Govers & Wortel, 2005; Royden & Papanikolaou, 2011; Suckale et al., 2009; Figure 2b). However, other studies (Halpaap et al., 2018; Pearce et al., 2012) are more consistent with a smooth, ramp-type structure between the subducting segments (Figure 2b). Tears within the subducting slab would also affect mantle flow beneath the WHSZ. This has been investigated with seismic anisotropy measurements (e.g., Evangelidis, 2017; Evangelidis et al., 2011; Hatzfeld et al., 2001; Olive et al., 2014; Paul et al., 2014; Schmid et al., 2004), but interpretations vary. Ultimately, the geometry of the subducting lithosphere beneath Greece requires further constraint.

3. Data and Methodology

To further examine the structure of the WHSZ, we have developed a new *P* wave tomography model using an adaptively parameterized inversion scheme. While several earlier studies employed similar approaches (e.g., Bijwaard et al., 1998; Hosa, 2008), both the methodology and data set for the current study have been updated and improved. Hansen et al. (2012, 2014) and Hansen and Nyblade (2013) provide descriptions of the inversion technique, but it is briefly described here.

Travel-time residuals for local, regional, and teleseismic phases are computed with respect to those from the ak135 Earth model (Kennett et al., 1995). Much of our data is provided by the global reprocessed ISC catalog (Figure 1; Engdahl et al., 1998), which provides travel-time residuals for a wide range of seismic phases (e.g., P, Pg, Pn, PKP, pP), thereby maximizing sampling of the Earth's structure. The global catalog used in the current study includes almost 25 million travel-time residuals from more than 530,000 earthquakes, which occurred between January 1964 and December 2013. Associated mean arrival time standard deviations vary between different seismic phases, but they average about 0.50 s across the full global data set (Engdahl et al., 1998; Gudmundsson et al., 1990).

Across Greece, seismic coverage is provided by the Hellenic Unified Seismic Network (HUSN; Figure 1). While data from many HUSN stations are available through the ISC, some stations are not reported. Temporary deployments, such as the MEDUSA (Multidisciplinary Experiments for Dynamic Understanding of Subduction under the Aegean Sea) and EGELADOS (Exploring the Geodynamics of Subducted Lithosphere Using an Amphibian Deployment of Seismographs) networks, are also an important source of seismic data for this region, but they are not included in the global catalog. Additionally, new data for many stations across Greece have become available since December 2013, when the global catalog ends. Much of these data are available either through the Data Management Center (DMC) operated by the Incorporated Research Institutions for Seismology (IRIS) or through the European Integrated Data Archive (EIDA), a distributed federation of datacenters in Europe. Access to restricted stations was provided

by the National Observatory of Athens. Therefore, the global ISC data set has been augmented with *P* wave travel-times from these additional sources.

The augmented Greece data set was manually picked, and the associated mean arrival time standard deviation is about 0.10 s. In total, the augmented data set includes about 88,000 travel-time residuals. Great care has been taken to combine the augmented data with the ISC catalog, and Figure S1 in the supporting information illustrates the consistency of the travel-time residuals between these different data sets. To balance the smaller but high-quality augmented data set against the global but somewhat noisier ISC catalog, the augmented data are given twice the weight in the tomographic inversion (Hansen et al., 2012, 2014; Kárason & van der Hilst, 2001; Li et al., 2008).

The full combined data set was inverted for a global model of mantle *P* wave structure using an iterative least squares approach as described by Li et al. (2008) and Hansen et al. (2012). Significant lateral variations in resolution can result from uneven seismic ray path coverage in the mantle; therefore, the tomographic approach employed constructs an adaptable grid based on the sampling density of the high-frequency data (e.g., Bijwaard et al., 1998; Kárason & van der Hilst, 2000). One or more cells from a base grid are combined until a minimum ray density in each cell is obtained, leading to an adaptive grid with finer spacing in regions with increased ray coverage. A variety of base grids and ray density thresholds were examined, and the finest-scale sampling was obtained using a base grid that is 0.7° in latitude and longitude and 45 km in depth with a minimum ray density of 900 hit counts (see Figures S2–S4 in the supporting information). This led to a total of ~760,000 sampled, adaptive cells in our associated inversion.

A full description of the associated sensitivity matrix calculations can be found in Kárason (2002) and Li et al. (2008). Briefly, short-period data with a center frequency of ~1 Hz are backprojected along ray paths computed in the ak135 reference model (Kennett et al., 1995), and weighted composite rays are used to reduce the size of the sensitivity matrix (Kárason & van der Hilst, 2001; Spakman & Nolet, 1988). Three-dimensional sensitivity kernels are approximated for long-period data using the approach of Kárason and van der Hilst (2001). This allows long wavelength structure to be constrained by low-frequency data without preventing smaller-scale structure from being resolved by short-period data. Additionally, an a priori 3-D crustal model (CRUST1.0; Laske et al., 2013) is incorporated into our inversion to account for crustal structure and to balance the crustal and upper mantle contributions to the misfit (Hansen et al., 2012; Li et al., 2008).

4. Results and Resolution

P wave velocity perturbations (δV_p) at selected mantle depths are shown in Figure 3, with cross-sections shown in Figure 4 and supporting information Figure S4. These results were obtained after 200 iterations of the inversion and correspond to a 94% reduction of the error function. The associated misfit vector decreased from 0.95 to 0.26 s, indicating the improvement in fit to the data between the starting model and the final model. At shallow depths (< ~50 km), the results are largely constrained by the a priori crustal model; therefore, we focus our interpretations on deeper portions of the model space. At 100-km depth, a fast seismic anomaly is observed along the eastern coast of Greece (Figure 3), consistent with estimates for the top of the slab (e.g., Bocchini et al., 2018; Gudmundsson & Sambridge, 1998). Fast velocities are also observed beneath northern Greece, the FYROM, and Bulgaria (Figures 1 and 3). Between ~150- and 225-km depth, the fast anomaly in eastern Greece is only observed along the southeastern and southern coasts of Peloponnese. Slower velocities are observed along the northeastern coast, extending down past the Gulf of Corinth (Features A and B, Figure 3). In this same depth range, fast velocities are also observed in northwestern central Greece, along ~21°E longitude, as well as along the western coast of Peloponnese, though the more southerly fast velocities do not extend to as great a depth (Features C and D, Figure 3). By 250- to 300-km depth, a broad-scale fast anomaly is again observed, underlying the Aegean Sea and extending northwestward (Figures 1 and 3). This feature continues to move to the northeast with depth.

Trench-perpendicular cross-sections further illustrate the structure beneath the WHSZ (Figure 4 and Figure S4a). Earthquake relocations from Halpaap et al. (2018) are also included. On Profiles 1–6, fast seismic velocities mark an anomaly that dips from the southwest to the northeast with depth; however, this anomaly is discontinuous between ~150 and 250 km. Following the trend of the dipping anomaly, the analyst has identified where the velocity structure changes from fast to slow (and vice versa) to estimate the western and eastern edges of the gap in the dipping structure (Feature A, Figure 4 and

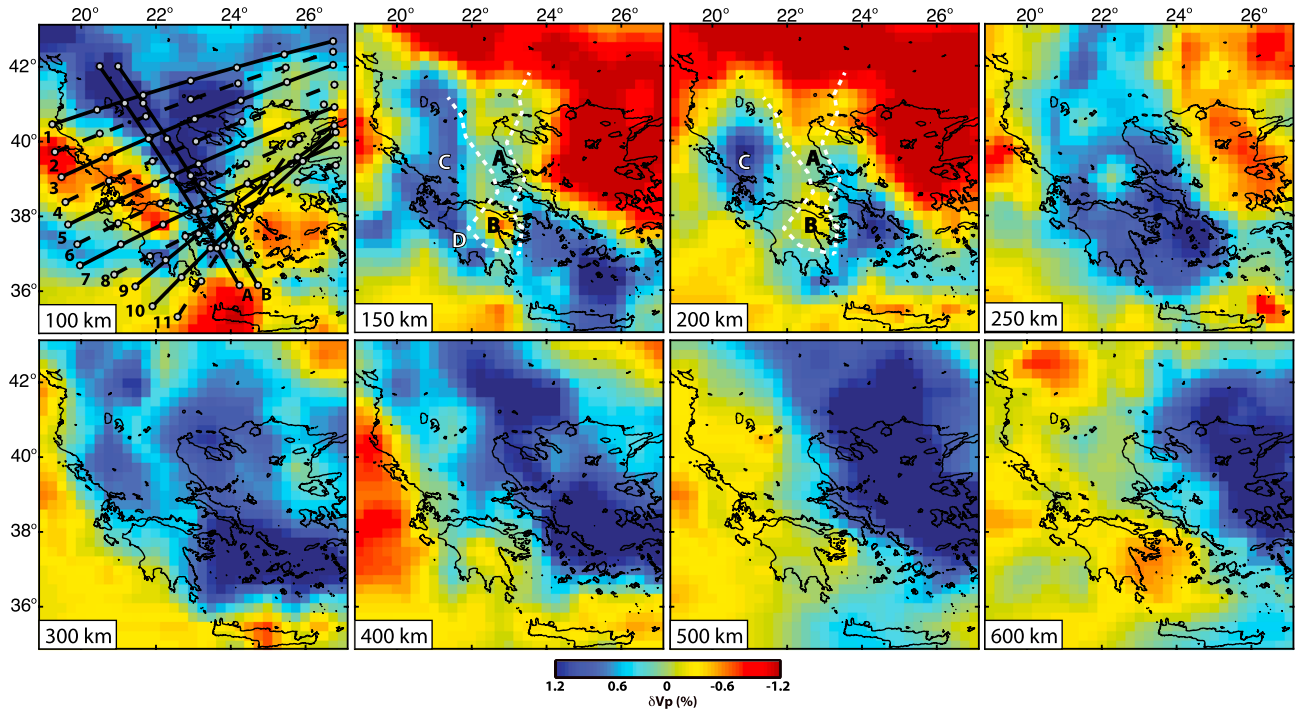

Figure 3. New *P* wave tomography model. *P* wave velocity perturbations (δV_p) are shown at selected mantle depths, with maps spaced more closely between 100 and 300 km since our interpretations focus on this portion of the model space. Locations of cross-sectional profiles are shown on the 100-km panel, with profiles marked by solid lines shown in Figure 4 (all profiles are provided in the supporting information). Trench-perpendicular profiles are sequentially numbered from north to south, and trench-parallel profiles are lettered from west to east. The dashed white lines on the 150- and 200-km panels show the 2-D projection of the interpreted slab tear and low-velocity "hole" (Features A and B), as described in the text. Features C and D correspond to fast velocities in northwestern-central Greece and along the western coast of Peloponnese.

Figure S4a). These locations are denoted with white tick marks on the cross-sectional profiles, and they have been projected onto the map view images shown in Figure 3. While few earthquakes occur along Profiles 1–3, it is interesting to note that Feature A occurs very close to the down-dip limit of seismicity on Profiles 4–6. The fast anomaly observed along ~21°E longitude in the map view images (Feature C, Figure 3) can also be seen on the southwestern portions of these profiles. Additionally, on Profiles 1–4, the fast velocities underlying the FYROM, northern Greece, and Bulgaria appear as a flat-lying anomaly at ~100- to 150-km depth. Further to the south, Profiles 7–11 instead show continuous fast velocities with depth, with an increased dip angle between ~60 and 80 km. This is coincident with a steeper and deeper pattern of seismicity (Halpaap et al., 2018). However, Profiles 7–9 also show a low-velocity "hole" (Feature B, Figures 3, 4 and Figure S4a) situated between dipping fast velocities to the northeast and another fast anomaly to the southwest, which is again associated with the fast velocities observed in the map view images (Feature D, Figure 3). Similar to Feature A on Profiles 1–6, the analyst has estimated the edges of Feature B on Profiles 7–9, which are again denoted with white tick marks on the cross-sectional images and which have been projected onto the maps in Figure 3. The dipping fast anomaly above Feature B is ~50-km thick between 100- and 200-km depth. Further south, cross sections along the tip of Peloponnese do not display this low-velocity hole, and the dipping fast anomaly is thicker (~100-km thick between 100- and 200-km depth; Profiles 10–11, Figure 4 and S4a).

Two trench-parallel profiles are also included (Figures 3, 4, and S4b) to further highlight the velocity structure. Between ~50- and 150-km depth, fast seismic velocities are fairly flat and continuous across the profiles, and it is worth noting that the earthquakes tend to cluster in this region (Halpaap et al., 2018). Further, the transition from continuous to discontinuous fast structure at ~150- to 250-km depth can also be seen near the southeastern portions of these profiles, including Feature B on Profiles 7–9 (Figure 4 and Figure S4a). Deeper earthquake hypocenters are also observed within the fast, continuous portion of the profiles.

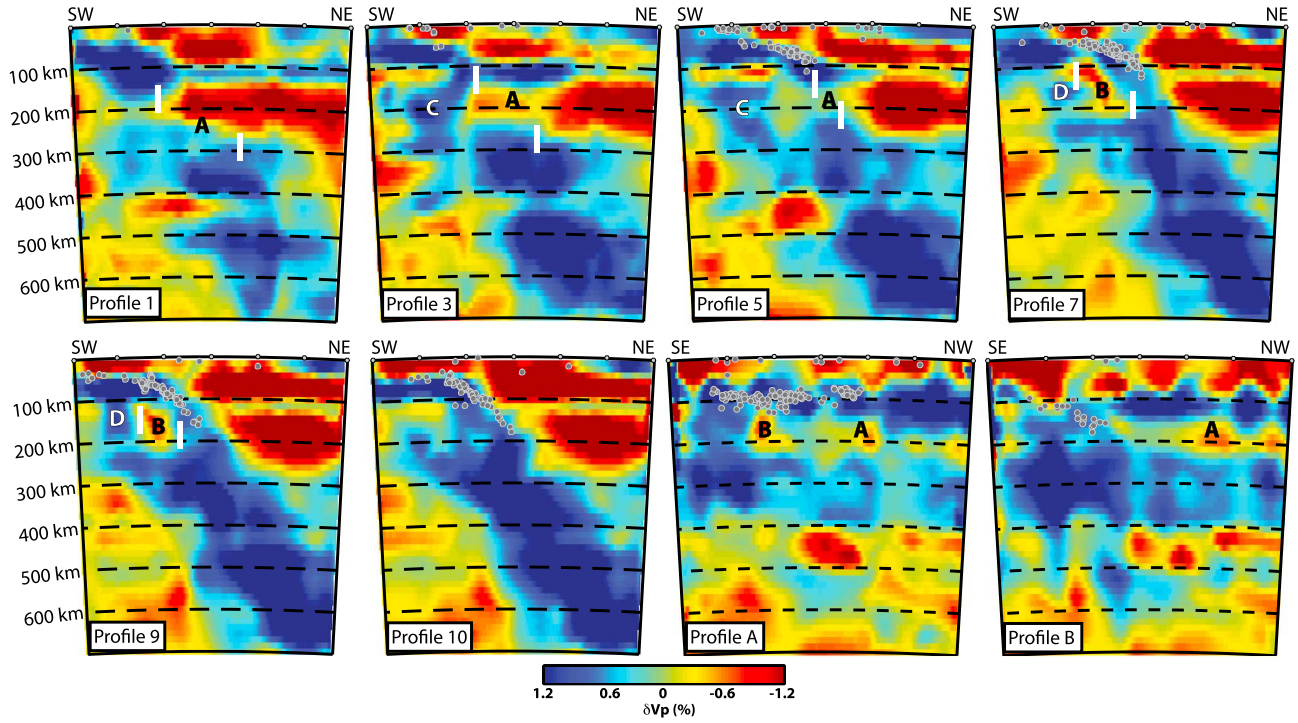

Figure 4. Selected cross sections through the new tomographic model. Locations are highlighted by solid profiles on Figure 3. White tick marks on Profiles 1–9 approximate the western and eastern edges of the slab tear and low-velocity "hole" (Features A and B), as described in the text. Features C and D correspond to fast velocities in northwestern-central Greece and along the western coast of Peloponnese (Figure 3). Gray dots show earthquake relocations from Halpaap et al. (2018), where all events within 0.2° are projected onto the cross section. Additional cross sections can be found in the supporting information.

A series of tests have been performed to assess model resolution. First, checkerboard tests are a common approach to assess lateral resolution. Our checkerboard tests have been constructed with an input pattern of 0.7°-wide anomalies with alternating ±2% δV_p variations. The anomalies have been projected onto the adaptive grid, and their thickness is equivalent to one cell (~45 km; Figure S4 in the supporting information). Each depth was tested individually (i.e., the anomalies outside the examined layer are set to zero). Synthetic travel-times were created and inverted using the same model parameterization as that used for the data. Additionally, noise was added to the synthetic travel-times as a Gaussian residual time error with a standard deviation of 0.26 s, which corresponds to the residual remaining in our model after inversion. This approach reproduces the same fit to the synthetic data as that provided by the actual model (Hansen et al., 2014; Hansen & Nyblade, 2013; Rawlinson et al., 2014). Lateral resolution in our model varies spatially (Figure 5), due to uneven station distribution throughout the study area, but the checkerboard pattern is generally well recovered at most upper mantle depths beneath Greece and adjacent regions. However, recovery rapidly decreases to the south-southwest offshore, where no station coverage is provided. Amplitude recovery varies between ~30-60%, largely due to regularization parameters used to stabilize the inversion. The amplitude recovery is even further reduced below ~700 km; therefore, we limit our interpretations to depths above this threshold.

In some cases, tightly spaced checkerboards may mask smearing effects (Rawlinson & Spakman, 2016); therefore, we also assess our model resolution with a sparse distribution of "spikes"—fast and slow anomalies—in the model space. As shown in Figure S5 in the supporting information, these spikes are comparable in size to Feature B (Figures 3 and 4). The results illustrate that our amplitude recovery is better in southern Greece, given the higher number of stations in this area (Figure 1). Lateral smearing is minimal, and vertical smearing is ~25–50 km. Additionally, since the checkerboard and distributed spike tests (Figures 5 and S5) are composed of anomalies that all have the same size, we also wanted to better assess the model resolution over the range of wavelengths present in our results. Therefore, we also performed a resolution test where our output model (Figures 3 and 4) was used as the "synthetic" input, and the results are shown in Figure S6 in the supporting information. As with our other synthetic tests, amplitudes in the recovered

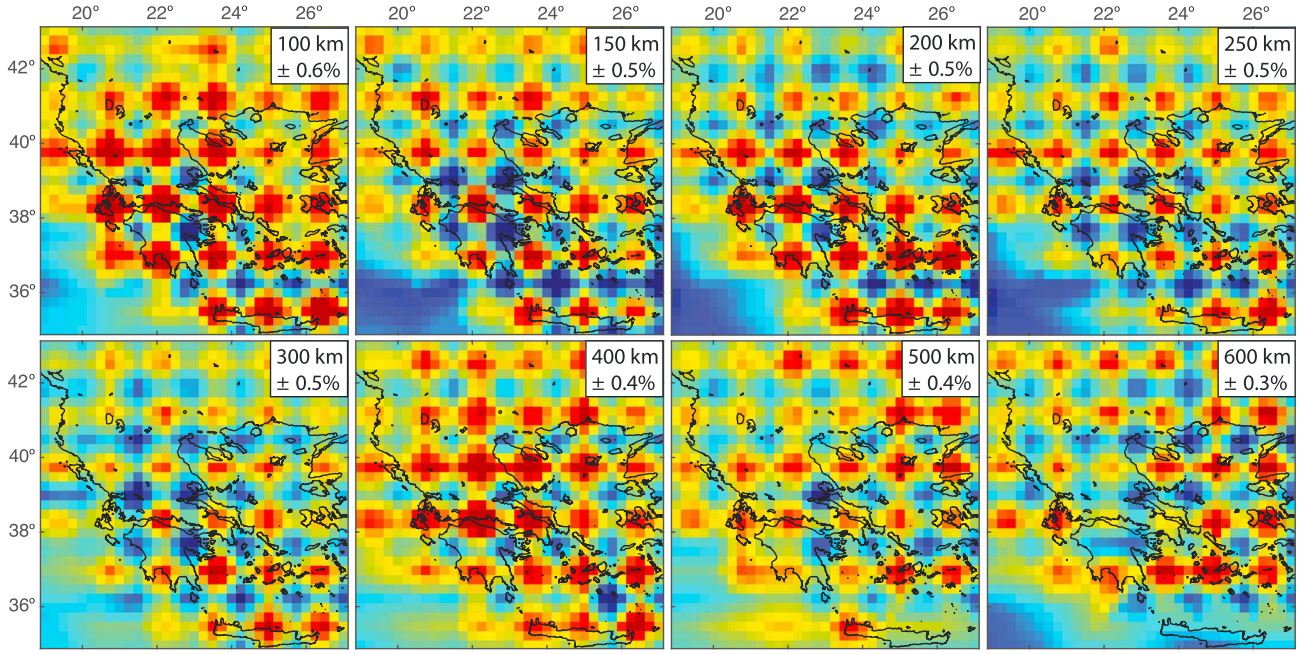

Figure 5. Checkerboard resolution tests at the same depths shown in Figure 3. Input pattern consists of 0.7°-wide anomalies with alternating ±2% δV_p variations, projected onto the adaptive grid. Note that the recovered pattern is plotted with different color scales depending on the panel.

model are lower than those in the input model. Some degree of lateral and vertical smearing is also observed, such as between Features C and D and the deeper fast anomaly to the northeast; however, the major features observed in our model (Figures 3 and 4) are well recovered (supporting information Figure S6).

To further assess specific structures in our model, additional tests were performed with synthetic anomalies along several of the examined profiles. Given the gridded parameterization, dipping interfaces must be approximated as stair-step structures, and as with the checkerboard tests, the synthetic anomalies are projected onto the adaptive grid. Within these constraints, the synthetics were constructed to match major observed features in the model as best as possible. Beneath northern Greece, our model shows a discontinuous, fast dipping anomaly (Figures 4 and S4a). The first set of synthetic tests (Figures 6a–6c) was constructed to examine this structure, using Profile 3 as a reference. All tests along this profile included the following synthetic anomalies. Between 50- and 125-km depth, fast anomalies with input amplitudes of +2% are included to represent the shallow mantle structure. These features extend ~524 km laterally across the ~698-km-long profile. Below 275-km depth, two additional fast anomalies laterally extend ~290 km across the lower portion of the profile. These anomalies have input amplitudes of +1.5% and are used to mimic the deeper, dipping structure. A ~233-km-long slow anomaly, centered at 160-km depth and with an input amplitude of −2%, is also included along the northeastern portion of the profile to match comparable slow velocities observed in this region on Profile 3 (Figure 4). It should be noted that different input amplitudes were tested for each of the synthetic anomalies, and more pronounced amplitudes generally lead to greater vertical smearing. However, such input amplitudes led to recovered anomalies whose amplitudes do not match those in the actual model. The employed input amplitudes provide the best match to the observed features (Figures 4 and 6). As with the other synthetic tests, Gaussian noise was added to the synthetic travel-times, which were inverted with the same model parameterization as that used for the data.

The structure between 125- and 275-km depth was varied to further assess the vertical resolution beneath northern Greece. First, as shown in Figure 6a, a ~115-km-wide connecting fast structure (input amplitude: +1.5%) is introduced to test whether a continuous dipping anomaly would be resolved, if present. As shown in the corresponding recovered model, such structure is resolvable; however, this does not match our observations (Figure 4). Instead, a synthetic model with a gap in the fast structure (Figure 6b), corresponding to Feature A (Figures 4 and S4a), better matches our tomographic images, despite the associated ~50 km of vertical smearing. A third test (Figure 6c) was also performed to assess the fast anomaly beneath northwestern-

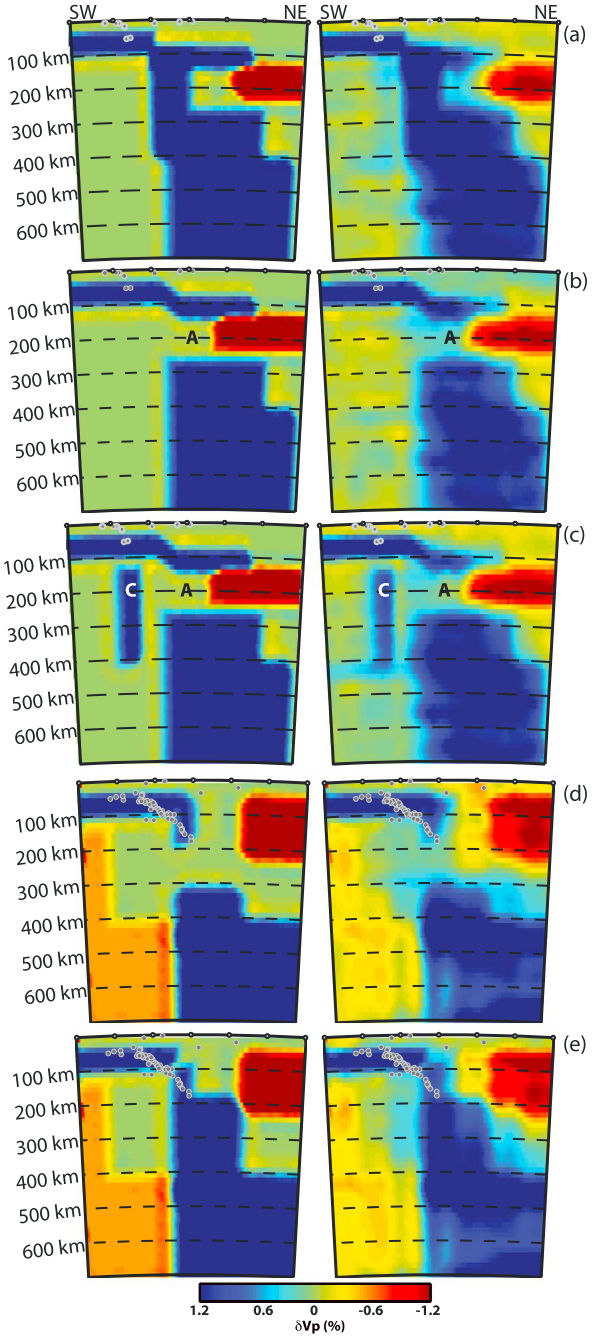

Figure 6. Input (left) and recovered (right) synthetic vertical resolution tests, plotted the same as Figure 4. (a) Synthetic test along Profile 3 beneath northern Greece (Figures 3 and 4). A connecting fast structure is introduced between 125 and 275 km to illustrate that such continuous structure would be resolved, if present. (b) Same as (a) but without the connecting fast anomaly to represent Feature A (Figures 4 and S4a). This synthetic test better matches our model (Figure 4) compared to (a). (c) Same as (b) but with a narrow vertical anomaly added to represent Feature C (Figures 4 and S4a). Results from (b) and (c) illustrate that this feature is not a smearing artifact of the model. (d) Synthetic test along Profile 10 beneath southern Greece (Figures 3 and 4). A 100-km gap in the fast dipping structure is introduced to illustrate that such discontinuous structure would be resolved, if present. (e) Same as (d) but now with a continuous fast structure that better matches our model observations (Figure 4).

central Greece (Feature C, Figures 4 and S4a). The synthetic tests in Figures 6a and 6b do not display such a feature, indicating that it is not a smearing effect of the model. This feature is best approximated by a ~65-km-wide synthetic anomaly (input amplitude: +1.5%), extending down to 400-km depth on the southwestern portion of the profile (Figure 6c). On some of the northern cross sections (Figure 4), Feature C appears to be separated from the overlying structure; therefore, we also include a ~50-km gap above Feature C to assess if this separation can be resolved. The corresponding recovered image indicates that this fast anomaly is a resolvable structure. A minor degree of smearing between Feature C and the deeper structure to the northeast is observed, but the gap above Feature C appears to be resolved. This is also supported by the recovery results shown in Figure S6b in the supporting information.

Beneath southern Greece, similar vertical resolution tests were also performed to assess whether a gap in the fast dipping structure (comparable to that seen in the north) would be resolved, if present. In this case, the ~670-km-long Profile 10 was used for reference (Figure 4). Between 50- and 200-km depth, two fast anomalies with input amplitudes of +2% and +1.2%, respectively, extend ~335 km laterally across the profile and are used to represent the shallow mantle structure. Below 300 km, two additional anomalies (input amplitudes: +1.5%) laterally extend ~390 km across the northeast portion of the profile and mimic the deeper, dipping structure. Two slow anomalies, with input amplitudes of −0.5% and widths of ~80 and ~250 km, respectively, are also included on the southwestern end of the profile, extending from 150- to 700-km depth. Additionally, a more pronounced slow anomaly (input amplitude: −1.5%) between 50- and 225-km depth extends ~170 km laterally on the northeastern portion of the profile. These slow anomalies match comparable slow velocities observed on Profile 10 (Figure 4). As with the synthetic tests discussed above (Figures 6a–6c), other input amplitudes were examined, but the employed amplitudes provide the best match to observed features in our model. The only difference between the synthetic tests shown in Figures 6d and 6e is the fast connecting structure between 200- and 300-km depth (input amplitude: +1.5%). These tests show that either structure is resolvable, but more importantly, if the fast dipping structure under Peloponnese were discontinuous (Figure 6d), similar to that seen beneath northern Greece, the resolution of our model is high enough that such a gap would be resolved. However, this does not match the observed structure (Figure 4), and a continuous fast anomaly with depth better matches our model beneath southern Greece (Figure 6e). Again, these results are further supported by the resolution test shown in Figure S6b.

5. Discussion

5.1. Subducting Slab Structure

The fast dipping structure beneath Greece imaged in our model is best attributed to the subducting slab. At shallow depths (< ~150 km), our tomographic results display a gently dipping anomaly, comparable to that imaged in previous local and regional tomographic studies (Halpaap et al., 2018; Lamara, 2014; Ligdas et al., 1990; Papazachos & Nolet, 1997; Tiberi et al., 2000). We do not observe any evidence for a trench-perpendicular tear across the CHSZ (Profiles A and B, Figure 4), suggesting continuous structure across the continental-

oceanic lithospheric boundary. This agrees well with recent studies by Pearce et al. (2012) and Halpaap et al. (2018), for instance, who suggest little to no offset of the lithosphere on either side of the KTF. Therefore, similar to these studies, we would advocate for a smooth ramp-like structure across the continent-ocean interface (Figure 2b). We also reiterate that the flat-lying fast anomaly between ~100- and 150-km depth on Profiles 1–4 underlies northern Greece and Bulgaria, and this feature is no longer observed once the profiles move offshore (Figures 4 and S4a). Therefore, this feature is attributed to the fast signature of the continental lithosphere in the overriding plate.

Within deeper portions of the WHSZ (>300 km), we observe continuous slab structure extending across the transition zone and into the lower mantle, consistent with broader-scale tomographic images for this area (e.g., Bijwaard et al., 1998; Hosa, 2008; Koulakov et al., 2009; Li et al., 2008; Piromallo & Morelli, 2003; Spakman et al., 1993; Zhu et al., 2015). While our resolution decreases below ~700-km depth, it is very likely that the subducting slab structure continues further into the lower mantle, as suggested by these earlier studies.

As previously stated, the major contribution of our new tomographic model is the improved resolution of structure between ~150- and 250-km depth, which bridges the gap between coverage provided by local and regional studies and that from broader-scale tomographic analyses. The discontinuous fast structure seen on Profiles 1–6 (Feature A, Figures 4 and S4a) is best attributed to a trench-parallel tear in the subducting lithosphere, similar to that shown in Figure 2a. This is in good agreement with previous studies that advocate for discontinuous or faded slab structure, particularly beneath northern Greece (Hosa, 2008; Koulakov et al., 2009; Pearce et al., 2012; Spakman et al., 1988, 1993; Zhu et al., 2015). Our model suggests that this trench-parallel tear is concentrated between ~150- and 250-km depth and extends southward to the Gulf of Corinth. That is, north of ~38.5°N latitude, the subducting slab appears to be completely detached.

As noted in section 2.0, convergence along the WHSZ has been associated with the subduction of several ocean basins (Dercourt et al., 1986; Ricou et al., 1998; Robertson et al., 1996). Nappe stacking suggests that while oceanic subduction was interspersed by continental units, continuous subduction has occurred along the Hellenic arc since the Cretaceous. This concept is generally referred to as a "single-slab" model, where continuously descending lithosphere from multiple stages of convergence results from back-stepping of the subduction between different microplates (e.g., Bocchini et al., 2018; Faccenna et al., 2003; Jolivet & Brun, 2010; Meier et al., 2004; van Hinsbergen et al., 2005). Our interpretation does not preclude continuous subduction along the WHSZ, but the presence of a trench-parallel tear does suggest additional considerations. For instance, Wong et al. (1997) and Wortel and Spakman (2000) argue that when continental lithosphere is subducted after a period of oceanic subduction, changes in the temperature and stress may lead to instabilities in the subducting lithosphere, creating a weak zone where a small, initial tear can develop in the subducting slab. Slab pull distribution would be affected by such a tear, concentrating the slab pull force into the portion of the slab that is still connected. Over time, this would cause the tear to propagate (Wortel & Spakman, 2000). In the WHSZ, north to south propagation of a trench-parallel tear could result from an initial disturbance in the subducting continental material beneath northern Greece that is then pulled by denser oceanic lithosphere subducting to the south (Royden & Papanikolaou, 2011; Wortel & Spakman, 2000).

In addition to the fast slab structure beneath eastern Greece, we also observe a fast anomaly beneath northwestern-central Greece, along ~21°E longitude (Feature C, Figure 3). Feature C extends down to ~300-400-km depth on Profiles 1–6 (Figures 3, 4, and S4a) and is located to the west-southwest of the interpreted tear. Our vertical resolution tests indicate that this is not a smearing artifact in the model (Figures 6a–6c). Similar fast velocities below northwestern-central Greece have been observed in some previous tomographic studies, based on both body and surface wave constraints (e.g., Hosa, 2008; Ligdas et al., 1990; Piromallo & Morelli, 2003; Salaün et al., 2012), though generally they have not been discussed. Given the degree of smearing indicated by our synthetic test results (Figures 6c and S6b), we cannot definitively determine whether Feature C is connected to the deeper slab or not. Also, on some profiles, Feature C appears to be separated from the overlying structure, and our synthetic tests indicate that this separation is resolvable (Figures 6c and S6b). Given its orientation and depth extent, Feature C is best interpreted as a lithospheric fragment, perhaps a remnant of the torn, detached slab. Similar structure has been seen, for example, beneath the Eastern Himalayan Syntaxis by Peng et al. (2016), where laterally varying subduction characteristics lead

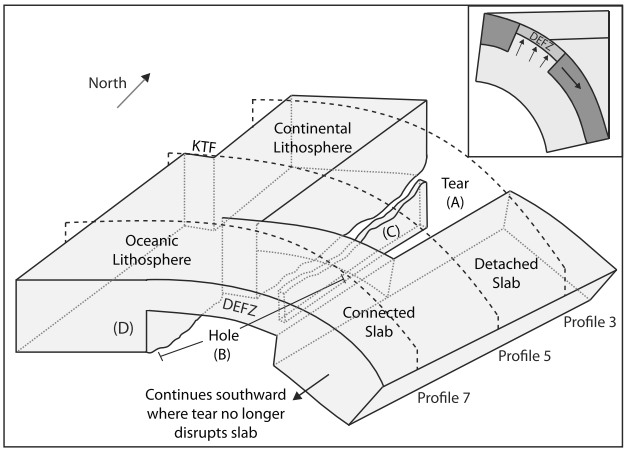

Figure 7. (inset) Stretching model for lithospheric detachment, modified from van de Zedde and Wortel (2001). The subducting lithosphere is thinned over a deformation zone (DEFZ), allowing hot mantle material to fill the gap and eventually leading to slab break-off. (main) Cartoon illustrating our interpretation of the slab structure (down to ~250-300-km depth; note: not drawn to scale), as inferred from our tomographic model. Black dashed arcs mark the approximate locations of representative profiles from Figure 4. Features labeled (A)–(D) correspond to the same labeled features on Figures 3 and 4. KTF: Kefalonia Transform Fault.

to tearing and fragmentation of the Indian lithosphere, and they suggest that the Hellenic system could be a comparable analogy.

An interesting change in the WHSZ structure is observed in the vicinity of the Gulf of Corinth. First, the dipping slab interface becomes continuous in this region, as seen on Profiles 7–11 (Figures 4 and S4a). It is worth noting that while some previous investigations have employed a similar methodology to that used in our study (e.g., Bijwaard et al., 1998; Hosa, 2008), their models do not resolve the subducting slab structure above ~250-km depth in this region (Figure S7 in the supporting information). Instead, continuous slab structure in those studies was inferred from the depth extent of seismicity; therefore, our model provides important new constraints on the slab structure in this area. The continuous structure is consistent with the single-slab model described previously (e.g., Faccenna et al., 2003; Jolivet & Brun, 2010; Meier et al., 2004; van Hinsbergen et al., 2005). However, a low-velocity hole is also observed beneath southern Greece (Feature B, Figures 3, 4, and S4), situated between fast velocities along the western coast of Peloponnese (Feature D) and the dipping slab to the northeast. Feature B is somewhat larger than the anomalies in our checkerboard resolution test (Figure 5), indicating it represents resolvable structure. This is further emphasized by the "spike" test shown in supporting information Figure S8 that mimics the slow anomaly and shows it is recovered by our model. We also note that similar slow structure in this area has been imaged by previous studies. For instance, the locally-focused *P* wave tomography model from Tiberi et al. (2000) shows pronounced slow velocities between ~140- and 200-km depth to the south-southwest of the Gulf of Corinth. The broader, Mediterranean-scale model from Piromallo and Morelli (2003) also indicates slow velocities between ~150- and 200-km depth beneath Peloponnese.

We interpret Feature B as marking the southernmost extent of the trench-parallel tear, where the surrounding lithosphere has become disrupted but has not completely detached. Feature B is bounded by the fast Ionian lithosphere on either side, including Feature D along the western coast of Peloponnese and the dipping slab to the northeast. This could be associated with a slab detachment mechanism similar to that suggested by van de Zedde and Wortel (2001; Figure 7 inset), where the lithosphere is stretched and thinned, eventually leading to slab break-off. As previously mentioned, supporting information Figure S6b suggests that Feature D is smeared toward the deeper slab to the northeast; therefore, a connection between Feature B and the underlying mantle is not well resolved. However, given our tomographic images along Profiles 7–9 (Figures 4 and S4), the fast-slow-fast pattern observed between Feature D, Feature B, and the dipping slab are best explained by the van de Zedde and Wortel (2001) mechanism. Past the southern coast of Peloponnese (Profiles 10–11, Figures 4 and S4), Feature B is no longer observed, and the subducting slab is thicker (~100-km thick between 100- and 200-km depth, compared to ~50-km thick further to the north), also consistent with this detachment mechanism. Therefore, we would argue that the tear has not extended into this region, similar to the conclusions of Spakman et al. (1988) and Meijer and Wortel (1996).

We note that Feature B is offset to the west compared to the trend of Feature A further to the north (Figure 3). As discussed in section 2, differential slab retreat beneath Greece is attributed to buoyancy differences between the subducting continental and oceanic lithosphere (e.g., Royden & Papanikolaou, 2011), and recent studies suggest that this transition is located near the KTF, in association with an abrupt change in seismicity (see section 5.2; Bocchini et al., 2018; Halpaap et al., 2018). Our results, and others (e.g., Halpaap et al., 2018; Pearce et al., 2012), suggest that this transition is associated with a ramp-type structure between the subducting segments (Figure 2b); therefore, nothing impedes the north to south propagation of the trench-parallel tear across the transition (Wortel & Spakman, 2000). The widely recognized westward retreat of the slab beneath Peloponnese is likely controlled by the geometry of the ramp. That is, the orientation of the ramp and the faster rollback associated with the oceanic slab causes a southwestward displacement of the trench along southern Greece (e.g., Halpaap et al., 2018), as perhaps evidenced by the 2008

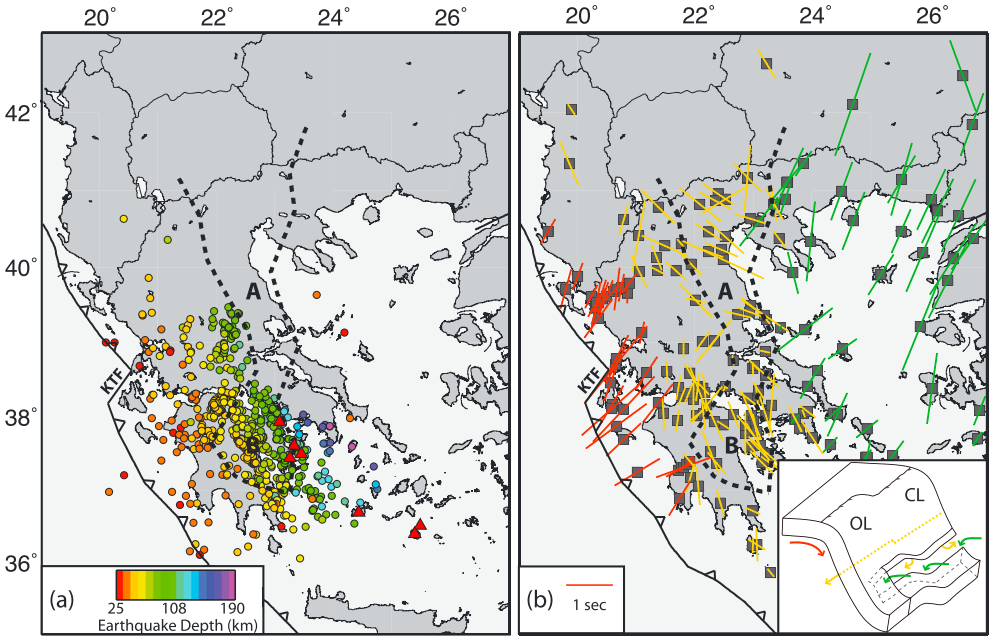

Figure 8. Maps showing (a) earthquake relocations from Halpaap et al. (2018) and (b) SKS splitting measurements from Evangelidis (2017, and references therein) in relation to the 2-D projection of the interpreted slab tear and low-velocity "hole" (Features A and B) from our tomographic model (black dashed line). In (a), earthquake epicenters (circles) are color coded by depth, and red triangles denote volcanoes. In (b), SKS splitting measurements at examined stations (gray squares) are oriented in the fast direction and are scaled to the delay time. Yellow markers denote trench-parallel measurements, while red and green markers denote subslab and wedge trench-perpendicular measurements, respectively, as interpreted by Evangelidis (2017). The inset shows a figure modified from Evangelidis (2017), illustrating the suggested mantle flow pattern (arrows), where the colors match those of the corresponding splitting measurements. CL: Continental Lithosphere; OL: Oceanic Lithosphere; KTF: Kefalonia Transform Fault.

right-lateral M_w 6.4 Movri earthquake in northwestern Peloponnese (Papadopoulos et al., 2010). Therefore, the orientation of the tear likely follows this westward retreat, as shown by the offset of Feature B.

Figure 7 summarizes our interpretation of the new tomographic model and the associated subducting slab structure. Offset along the KTF between the northern, continental and southern, oceanic segments of the subduction zone is inferred from earlier studies that examined shallower structure along the WHSZ (e.g., Kahle & Mueller, 1998; Hollenstein et al., 2008; Royden & Papanikolaou, 2011). The subducting lithosphere initially has a shallow dip, and the transition from continental to oceanic lithosphere is a smooth ramp, with no trench-perpendicular tear between these segments. Further to the east and north of ~38.5°N latitude, the subducting slab is torn and completely detached by a trench-parallel tear (Feature A). Feature C is best interpreted as a lithospheric fragment on the western side of the tear. As discussed previously, it is unclear whether Feature C is connected to the deeper slab, and some profiles (Figures 4 and S4) suggest Feature C is not connected to the shallower subducting lithosphere. Therefore, it is included as a separate, disconnected feature for the purposes of our cartoon interpretation. To the south of the Gulf of Corinth, the slab is continuous; however, the slab beneath Peloponnese is disrupted by the southern end of the tear (Feature B). This leads to lithospheric thinning, but the slab has not been completely detached. The slab is also retreating to the west in this area, given the drag of the dense oceanic lithosphere, causing the orientation of the tear to change as it propagates southward. This disturbance continues to the southern coast of Peloponnese, where the slab is no longer disrupted by the tear.

5.2. Relation to Seismicity

Our tomographic images and the geometry of the interpreted trench-parallel tear are well correlated with seismicity; therefore, our results may provide insight into earthquake patterns along the WHSZ. South of the KTF and just north of the Gulf of Corinth, the down-dip limit of seismicity is constrained between ~60- and 80-km depth (Figure 8a; Halpaap et al., 2018). As seen from our cross-sectional profiles

(Figures 4 and S4a), the gap in the fast dipping slab structure (Feature A) occurs just below this point. Laterally, the approximate western edge of the tear correlates well with the termination of seismicity (Figure 8a). Therefore, in this region, we suggest that the down-dip limit of seismicity is controlled by the trench-parallel tear. That is, the detached lithosphere imaged by our tomography has removed the associated slab pull force, which may be associated with intermediate-depth earthquakes. It is worth noting that the trench-parallel tear also appears to continue to the north of the KTF, where few earthquakes occur (Bocchini et al., 2018; Halpaap et al., 2018). As noted in the previous section, our tomographic results show no evidence for a trench-perpendicular tear in this region; therefore, we would advocate that the abrupt change in seismicity across the KTF is best attributed to compositional differences between the subducting continental and oceanic lithosphere, similar to that suggested by Halpaap et al. (2018) and Bocchini et al. (2018). Further, it is interesting that no earthquakes occur in the detached portion of the slab (Figures 4 and S4a). Many mechanisms have been proposed for deep-focus earthquakes (>300 km), as reviewed, for instance, by Green and Houston (1995) and Houston (2015). While this topic is beyond the scope of the current study, it has been suggested that a long episode of slow subduction prior to ~5 Ma may be responsible for the aseismic slab at depth beneath the WHSZ (Shaw & Jackson, 2010).

Within and to the south of the Gulf of Corinth, the seismicity extends to greater depths, reaching ~190 km along the eastern coast of Peloponnese (Figure 8a; Bocchini et al., 2018; Halpaap et al., 2018). The corresponding tomographic images (Profiles 7–11, Figures 4 and S4a) again suggest continuous slab structure in this region, coincident with the deeper and steeper Wadati-Benioff zone. That being said, it is worth noting that Rontogianni et al. (2011) suggested that stress inversions for events in this area are consistent with a slab tear. As discussed in section 5.1, Feature B likely indicates the southernmost extent of the trench-parallel tear, and while the slab is thinned in this area, it has not yet been detached. Given this, some events in Peloponnese may reflect stress conditions associated with the interpreted disturbance at the southern edge of the tear (Rontogianni et al., 2011).

As discussed in section 2, many tomographic studies, including the current one, suggest that the slab extends across the transition zone and well into the lower mantle beneath the WHSZ (Bijwaard et al., 1998; Bourova et al., 2005; Di Luccio & Pasyanos, 2007; Endrun et al., 2008; Hosa, 2008; Konstantinou & Melis, 2008; Koulakov et al., 2009; Li et al., 2008; Pasyanos & Walter, 2002; Piromallo & Morelli, 2003; Salaün et al., 2012; Schmid et al., 2006; Spakman et al., 1988, 1993; Zhu et al., 2015). However, seismicity is constrained to the upper ~200 km within this region (Bocchini et al., 2018; Brüstle, 2012; Durand et al., 2014; Galanis et al., 2006; Halpaap et al., 2018; Karakonstantis & Papadimitriou, 2010; Papazachos et al., 2000). If the slab is continuous below 200-km depth, as shown on Profiles 7–11 (Figures 4 and S4a), why are no earthquakes observed within the deeper subducting lithosphere?

Several suggestions have been put forth to explain this apparent discrepancy between the tomographically imaged slab and the depth extent of the seismicity. For instance, Papadopoulos (1997) suggested that tomographic studies may be imaging earlier, non-assimilated lithospheric remnants associated with earlier phases of subduction and that the resolution of these models was not high enough to distinguish between different segments, indicating that the subducted slab is not actually continuous and that seismicity defines the maximum depth of the currently descending slab. We have tested this hypothesis with our vertical resolution models. Based on radiometric data, Papadopoulos (1989, 1997) suggest a ~3-Ma time difference between Late Miocene (14–7 Ma) and Plio-Quaternary (4 Ma–present) phases of volcanism in the Aegean region, which they attribute to different phases of subduction. Using their reported 3.2 cm/year subduction rate, this would indicate a ~100-km separation between these two subducted segments; therefore, we introduced a ~100-km gap in the fast slab structure in our vertical resolution test shown in Figure 6d. However, as previously discussed, if such a gap were present in the subducting slab structure, it would be resolved by our model. Therefore, the difference between the seismicity and the imaged slab structure does not appear to be a resolution issue, and we advocate for continuous slab beneath southern Greece. Again, this idea is consistent with the single-slab model discussed previously (e.g., Bocchini et al., 2018; Faccenna et al., 2003; Jolivet & Brun, 2010; Meier et al., 2004; van Hinsbergen et al., 2005).

It has also been suggested that the seismically fast velocities below 200-km depth are not associated with subducting lithosphere at all. Based on work by Doglioni et al. (2009), Agostini et al. (2009) suggest that deeper, more rigid mantle material, characterized by faster seismic velocities compared to shallower mantle, could

be upraised by slab suction forces associated with the northeast-oriented subduction zone. This could cause a "ghost slab" to be imaged beneath the WHSZ, but the termination in seismicity at ~200-km depth would be due to the fact that the slab was actually missing below this area. If this were the case, it would be expected that such suction would lead to comparable ghost slab structure along-strike of the WHSZ, which is not observed by our model. Further, this mechanism cannot explain the abrupt change in the down-dip limit of seismicity on either side of the Gulf of Corinth (Figure 8a). Additionally, below ~300 km, the fast seismic anomalies trend to the northeast with depth (Figure 3), as would be expected from subducting lithosphere moving further into the mantle. Therefore, this mechanism is not supported by our tomographic results.

Alternatively, numerous studies have suggested that intermediate-depth seismicity is due to petrologic changes and dehydration processes within subducting slabs (e.g., Hacker et al., 2003; van Keken et al., 2011), and several investigations have suggested that these characteristics control the down-dip limit of seismicity beneath Greece (e.g., Brüstle, 2012; Halpaap et al., 2018; Wortel et al., 1990). In other words, the extent of the Wadati-Benioff zone does not reflect the termination of the subducting lithosphere but rather where the slab has become completely dehydrated. Comparable interpretations have been made for the subducting Cocos plate, for instance, where tomography indicates the subducting lithosphere extends to ~550 km but seismicity ends at ~150 km (e.g., Husker & Davis, 2009; Pardo & Suarez, 1995). Dehydration may also play an important role in magma generation and volcanism beneath southern Greece (Halpaap et al., 2018), which is described further in the next section.

To summarize, we suggest that the down-dip limit of seismicity north of the Gulf of Corinth is controlled by the geometry of the trench-parallel tear imaged in our tomographic model, where the slab is completely detached. Further to the south, the slab is thinned by the tear, but both the continuous fast, dipping structure and the seismicity pattern indicate that the slab has not been detached in this region. Instead, the deeper down-dip limit of seismicity in Peloponnese is attributed to dehydration processes in the subducting lithosphere. Our tomographic interpretation can explain the abrupt change in the depth extent of WHSZ earthquakes across the Gulf of Corinth.

5.3. Relation to Mantle Flow, Anisotropy, and Volcanism

As noted in section 2, tears in the subducting lithosphere would influence mantle flow beneath the WHSZ, and this has been investigated with seismic anisotropy measurements (e.g., Evangelidis, 2017; Evangelidis et al., 2011; Hatzfeld et al., 2001; Olive et al., 2014; Paul et al., 2014; Schmid et al., 2004). In Figure 8b, we show how the approximate geometry of the trench-parallel tear compares to SKS splitting measurements compiled from previous investigations. Some interesting comparisons can be made. For instance, the tear appears to correlate with roughly trench-parallel fast-splitting directions, while more trench-perpendicular fast directions are observed to the east and west. Evangelidis (2017) suggested that the trench-parallel splitting measurements are consistent with subslab mantle flow parallel to a smooth, ramp-like connection between the subducting continental and oceanic lithosphere at depth and do not indicate a trench-perpendicular tear. These interpretations well match those from the current study. We further suggest that escape flow through the trench-parallel tear could also lead to a diffused converging pattern of splitting observations, especially within the northern, wider portions of Feature A (Figure 8b). Near Feature B, the trench-parallel splitting directions are more consistent, which may reflect flow beneath the thinned slab, directed toward the southern end of the tear. This could also explain why Feature B has a somewhat more pronounced low-velocity signature than Feature A further to the north (Figure 3); however, we also note that there are more seismic stations across Peloponnese compared to the eastern coast of Greece (Figure 1), so the amplitude difference between these two areas may also just be due to the fact that we have more sampling of the structure in Peloponnese (Figures S2 and S5 in the supporting information). The trench-perpendicular splitting measurements in western Greece have been interpreted to reflect subslab mantle flow, while those in eastern Greece and the Aegean are associated with flow in the mantle wedge, which could also be directed through the trench-parallel tear (Figure 8b). Similar anisotropy patterns in the eastern Hellenic Subduction Zone between Crete and Rhodes have been interpreted to reflect such structure (Evangelidis, 2017).

Another interesting comparison can be made between our tomographic model and the location of volcanic centers. While there is no recent volcanism north of the Gulf of Corinth, Plio-Quaternary alkaline volcanic rocks are found in eastern central Greece (e.g., Papadopoulos, 1989), and these may be associated with

subduction prior to the detachment of the slab. Further south, four volcanoes in the vicinity of northeastern Peloponnese mark the northern end of the Hellenic volcanic arc, and these volcanoes all cluster around the eastern side of Feature B (Figure 8a). Wortel and Spakman (1992) suggested that the geometry of the subducting slab (whether continuous or detached) strongly influences the distribution and nature of Mediterranean volcanism. Further, Pe-Piper and Piper (2007) have noted that the geochemical signature of volcanic rocks in the Aegean region cannot be simply explained by post-collisional extension and instead require partial melting of the lithospheric mantle and lower crust associated with advection of the asthenosphere related to tears in the subducting slab. The Peloponnese volcanoes display different eruptive behavior and magmatic compositions compared to volcanoes in the central and eastern portions of the Hellenic arc (e.g., D'Alessandro et al., 2010; Pe-Piper & Piper, 2007). Therefore, volcanism in Peloponnese may be influenced by the southern end of the tear. Dehydration of the subducting slab in this area, as discussed above in relation to the down-dip limit of seismicity, may also help to promote magmatism. For example, Halpaap et al. (2018) found high Vp/Vs ratios at ~80-km depth beneath the western Hellenic arc volcanoes, and such velocity ratios are typically associated with water-rich fluids or melts. Water released from the subducting lithosphere may hydrate the overlying mantle wedge, also promoting partial melting in this area.

6. Conclusions

We have generated a new *P* wave velocity model for the WHSZ using an adaptively parameterized tomographic approach. The employed data set and methodology bridges the gap between coverage provided by local and regional studies and that from broader-scale tomographic analyses, highlighting the subducting slab structure between ~150- and 250-km depth. North of ~38.5°N latitude, our tomographic model suggests that the slab has been detached by a trench-parallel tear. To the south and beneath Peloponnese, a low-velocity hole marks the southern end of the tear, where the slab has been thinned but not yet detached. The down-dip limit of seismicity in central Greece well correlates with the edge of the interpreted tear, while the continuous and steeper fast slab structure in southern Greece well matches the pattern of seismicity down to ~200-km depth. While the slab continues past this point, earthquakes terminate, likely due to dehydration of the subducting lithosphere. The southern end of the tear is also coincident with volcanic centers in southeastern Greece and may contribute to volcanism in this region. The trench-parallel tear does not extend past the southern coast of Peloponnese.

Acknowledgments
We thank Felix Halpaap for providing earthquake relocations from his 2018 study and two anonymous reviewers for their thorough critiques of this manuscript. We also thank the IRIS DMC and EIDA for providing data-handling assistance. Specifically, data from regional seismic networks XS (doi: 10.7914/SN/XS_2006), YF, GE (doi: 10.14470/TR560404), HL (doi: 10.7914/SN/HL), HT (doi: 10.7914/SN/HT), and MN (doi: 10.13127/SD/fBBBtDtd6q) were sourced from the IRIS DMC, and data from regional networks HL (doi: 10.7914/SN/HL), HT (doi: 10.7914/SN/HT), HA (doi: 10.7914/SN/HA), HP (doi: 10.7914/SN/HP), HC (doi: 10.7914/SN/HC), CQ (doi: 10.7914/SN/CQ), Z3 (doi: 10.14470/M87550267382), and CL (doi: 10.15778/RESIF.CL) were sourced from EIDA. Funding for this research was provided by the Fulbright Foundation in Greece. Some figures were generated with Generic Mapping Tools (Wessel & Smith, 1995).

References

Agostini, S., Doglioni, C., Innocenti, F., Manetti, P., & Tonarini, S. (2009). On the geodynamics of the Aegean rift. *Tectonophysics*, *488*, 7–21.

Bell, R. E., McNeill, L. C., Bull, J. M., Henstock, T. J., Collier, R. E. L., & Leeder, M. R. (2009). Fault architecture, basin structure and evolution of the Gulf of Corinth rift, Central Greece. *Basin Research*, *21*(6), 824–855. https://doi.org/10.1111/j.1365-2117.2009.00401.x

Bijwaard, H., Spakman, W., & Engdahl, E. R. (1998). Closing the gap between regional and global travel time tomography. *Journal of Geophysical Research*, *103*(B12), 30,055–30,078. https://doi.org/10.1029/98JB02467

Bird, P. (2003). An updated digital model of plate boundaries. *Geochemistry, Geophysics, Geosystems*, *4*(3), 1027. https://doi.org/10.1029/2001GC000252

Bocchini, G. M., Brüstle, A., Becker, D., Meier, T., van Keken, P. E., Ruscic, M., et al. (2018). Tearing, segmentation, and backstepping of subduction in the Aegean: New insights from seismicity. *Tectonophysics*, *734-735*, 96–118. https://doi.org/10.1016/j.tecto.2018.04.002

Bohnhoff, M., Harjes, H. P., & Meier, T. (2005). Deformation and stress regimes in the Hellenic subduction zone from focal mechanisms. *Journal of Seismology*, *9*(3), 341–366. https://doi.org/10.1007/s10950-005-8720-5

Bohnhoff, M., Makris, J., Papanikolaou, D., & Stavrakakis, G. (2001). Crustal investigation of the Hellenic subduction zone using wide aperture seismic data. *Tectonophysics*, *343*(3-4), 239–262. https://doi.org/10.1016/S0040-1951(01)00264-5

Bourova, E., Kassaras, I., Pedersen, H., Yanovskaya, T., Hatzfeld, D., & Kiratzi, A. (2005). Constraints on absolute S velocities beneath the Aegean Sea from surface wave analysis. *Geophysical Journal International*, *160*(3), 1006–1019. https://doi.org/10.1111/j.1365-246X.2005.02565.x

Brüstle, A. (2012). Seismicity of the Eastern Hellenic Subduction Zone, PhD thesis, University of Bochum, Germany.

Carminati, E., Wortel, M. J. R., Spakman, W., & Sabadini, R. (1998). The role of slab detachment processes in the opening of the western-Central Mediterranean basins: Some geological and geophysical evidence. *Earth and Planetary Science Letters*, *160*(3-4), 651–665. https://doi.org/10.1016/S0012-821X(98)00118-6

Chousianitis, K., Ganas, A., & Evangelidis, C. P. (2015). Strain and rotation rate patterns of mainland Greece from continuous GPS data and comparison between seismic and geodetic moment release. *Journal of Geophysical Research: Solid Earth*, *120*, 3909–3931. https://doi.org/10.1002/2014JB11762

Clément, C., Hirn, A., Charvis, P., Sachpazi, M., & Marnelis, F. (2000). Seismic structure and the active Hellenic subduction in the Ionian Islands. *Tectonophysics*, *329*(1-4), 141–156. https://doi.org/10.1016/S0040-1951(00)00193-1

D'Alessandro, W., Brusca, L., Martelli, M., Rizzo, A., & Kyriakopoulos, K. (2010). Geochemical characterization of natural gas manifestations in Greece. Bulletin of the Geological Society of Greece: Proceedings of the 12th International Congress, Patras, Greece.

de Voogd, B., Truffert, C., Chamot-Rooke, N., Huchon, P., Lallemant, S., & Le Pichon, X. (1992). Two-ship deep seismic soundings in the basins of the eastern Mediterranean Sea (Pasiphae cruise). *Geophysical Journal International*, *109*(3), 536–552. https://doi.org/10.1111/j.1365-246X.1992.tb00116.x

Del Ben, A., Mocnik, A., Volpi, V., & Karvelis, P. (2015). Old domains in the South Adria plate and their relationship with the West Hellenic front. *Journal of Geodynamics*, *89*, 15–28.

Dercourt, J., Zonenshain, L. P., Ricou, L.-E., Kazmin, V. G., Le Pichon, X., Knipper, A. L., et al. (1986). Geological evolution of the Tethys belt from the Atlantic to the Pamirs since the Lias. *Tectonophysics*, *123*(1-4), 241–315. https://doi.org/10.1016/0040-1951(86)90199-X

Di Luccio, F., & Pasyanos, M. (2007). Crustal and upper-mantle structure in the eastern Mediterranean from the analysis of surface wave dispersion curves. *Geophysical Journal International*, *169*(3), 1139–1152. https://doi.org/10.1111/j.1365-246X.2007.03332.x

Doglioni, C., Tonarini, S., & Innocenti, F. (2009). Mantle wedge asymmetries along opposite subduction zones. *Lithos*, *113*(1-2), 179–189. https://doi.org/10.1016/j.lithos.2009.01.012

Durand, V., Bouchon, M., Floyd, M. A., Theodulidis, N., Marsan, D., Karabulut, H., & Schmittbuhl, J. (2014). Observation of the spread of slow deformation in Greece following the breakup of the slab. *Geophysical Research Letters*, *41*, 7129–7134. https://doi.org/10.1002/2014GL061408

Endrun, B., Ceranna, L., Meier, T., Bohnhoff, M., & Harjes, H. P. (2005). Modeling the influence of Moho topography on receiver functions: A case study from the central Hellenic subduction zone. *Geophysical Research Letters*, *32*, L12311. https://doi.org/10.1029/2005GL023066

Endrun, B., Meier, T., Lebedev, S., Bohnhoff, M., Stavrakakis, G., & Harjes, H. P. (2008). S velocity structure and radial anisotropy in the Aegean region from surface wave dispersion. *Geophysical Journal International*, *174*(2), 593–616. https://doi.org/10.1111/j.1365-246X.2008.03802.x

Engdahl, E. R., van der Hilst, R. D., & Buland, R. (1998). Global teleseismic earthquake relocation with improved travel times and procedures for depth determination. *Bulletin of the Seismological Society of America*, *88*, 722–743.

Evangelidis, C. P. (2017). Seismic anisotropy in the Hellenic subduction zone: Effects of slab segmentation and subslab mantle flow. *Earth and Planetary Science Letters*, *480*, 97–106.

Evangelidis, C. P., Liang, W.-T., Melis, N. S., & Konstantinou, K. I. (2011). Shear wave anisotropy beneath the Aegean inferred from SKS splitting observations. *Journal of Geophysical Research*, *116*, B04314. https://doi.org/10.1029/2010JB007884

Faccenna, C., Jolivet, L., Piromallo, C., & Morelli, A. (2003). Subduction and the depth of convection in the Mediterranean mantle. *Journal of Geophysical Research*, *108*(B2), 2099. https://doi.org/10.1029/2001JB001690

Finetti, I., Papanikolaou, D., Del Ben, A., & Karvelis, P. (1991). Preliminary geotectonic interpretation of the East Mediterranean chain and the Hellenic arc. *Bulletin of the Geological Society of Greece*, *25*, 509–526.

Finetti, I. R. & Del Ben, A. (2005). Crustal tectono-stratigraphic setting of the Adriatic Sea from new CROP seismic data. In I. R. Finelli (Ed.), *Deep Seismic Exploration of the Central Mediterranean and Italy* (Chap. 23, 519–548). Amsterdam: Elsevier.

Galanis, O., Papazachos, C., Scordilis, E., & Hatzidimitriou, P. (2006). Improved earthquake locations in Greece using the DD algorithm and a 3D velocity model, First European Conference on Earthquake Engineering and Seismology, 810.

Gesret, A., Laigle, M., Diaz, J., Sachpazi, M., Charalampakis, M., & Hirn, A. (2011). Slab top dips resolved by teleseismic converted waves in the Hellenic subduction zone. *Geophysical Research Letters*, *38*, L20304. https://doi.org/10.1029/2011GL048996

Govers, R., & Wortel, M. (2005). Lithospheric tearing at {STEP} faults: Response to edges of subduction zones. *Earth and Planetary Science Letters*, *236*(1-2), 505–523. https://doi.org/10.1016/j.epsl.2005.03.022

Green, H. W., & Houston, H. (1995). The mechanics of deep earthquakes. *Annual Review of Earth and Planetary Sciences*, *23*(1), 169–213. https://doi.org/10.1146/annurev.ea.23.050195.001125

Gudmundsson, O., Davies, J. H., & Clayton, R. W. (1990). Stochastic analysis of global traveltime data: Mantle heterogeneity and random errors in the ISC data. *Geophysical Journal International*, *102*(1), 25–43. https://doi.org/10.1111/j.1365-246X.1990.tb00528.x

Gudmundsson, O., & Sambridge, M. (1998). A regionalized upper mantle (RUM) seismic model. *Journal of Geophysical Research*, *103*(B4), 7121–7136. https://doi.org/10.1029/97JB02488

Hacker, B. R., Peacock, S. M., Abers, G. A., & Holloway, S. D. (2003). Subduction factory 2: Are intermediate-depth earthquakes in subducting slabs linked to metamorphic dehydration reactions? *Journal of Geophysical Research*, *108*(B1), 2030. https://doi.org/10.1029/2001JB001129

Halpaap, F., Rondenay, S., & Ottemöller, L. (2018). Seismicity, deformation, and metamorphism in the Western Hellenic subduction zone—New constraints from tomography. *Journal of Geophysical Research: Solid Earth*, *123*, 3000–3026. https://doi.org/10.1002/2017JB015154

Hansen, S. E., Graw, J. H., Kenyon, L. M., Nyblade, A. A., Wiens, D. A., Aster, R. C., et al. (2014). Imaging the Antarctic mantle using adaptively parameterized P-wave tomography: Evidence for heterogeneous structure beneath West Antarctica. *Earth and Planetary Science Letters*, *408*, 66–78. https://doi.org/10.1016/j.epsl.2014.09.043

Hansen, S. E., & Nyblade, A. A. (2013). The deep seismic structure of the Ethiopia/Afar hotspot and the African superplume. *Geophysical Journal International*, *194*, 118–124.

Hansen, S. E., Nyblade, A. A., & Benoit, M. H. (2012). Mantle structure beneath Africa and Arabia from adaptively parameterized *P*-wave tomography: Implications for the origin of Cenozoic afro-Arabian tectonism. *Earth and Planetary Science Letters*, *319-320*, 23–34. https://doi.org/10.1016/j.epsl.2011.12.023

Hatzfeld, D., Karagianni, E., Kassaras, I., Kiratzi, A., Louvari, E., Lyon-Caen, H., et al. (2001). Shear wave anisotropy in the upper mantle beneath the Aegean related to internal deformation. *Journal of Geophysical Research*, *106*(B12), 30737–30753. https://doi.org/10.1029/2001JB000387

Hollenstein, C., Müller, M. D., Geiger, A., & Kahle, H. G. (2008). Crustal motion and deformation in Greece from a decade of GPS measurements, 1993–2003. *Tectonophysics*, *449*(1-4), 17–40. https://doi.org/10.1016/j.tecto.2007.12.006

Hosa, A. M. (2008). Imaging of the Hellenic subduction zone by seismic tomography. *BSc thesis*, Massachusetts Institute of Technology, Cambridge.

Houston, H. (2015). Deep earthquakes. *Treatise on Geophysics*, *4*, 329–354.

Husker, A., & Davis, P. M. (2009). Tomography and thermal state of the Cocos plate subduction beneath Mexico City. *Journal of Geophysical Research*, *114*, B04306. https://doi.org/10.1029/2008JB006039

Jolivet, L., & Brun, J. P. (2010). Cenozoic geodynamic evolution of the Aegean. *International Journal of Earth Sciences*, *99*(1), 109–138. https://doi.org/10.1007/s00531-008-0366-4

Kahle, H.-G., & Mueller, S. (1998). Structure and dynamics of the Eurasian-African/Arabian plate boundary system: Objectives, tasks, and resources of the WEGENER group. *Journal of Geodynamics*, *25*(3-4), 303–325. https://doi.org/10.1016/S0264-3707(97)00033-1

Karakonstantis, A., & Papadimitriou, P. (2010). Earthquake relocation in Greece using a unified and homogenized seismological catalogue. *Bulletin of the Geological Society of Greece*, *43*, 2043–2052.

Kárason, H. (2002). Constraints on mantle convection from seismic tomography and flow modeling. *Ph.D. Thesis*, Massachusetts Institute of Technology.

Kárason, H., & van der Hilst, R. D. (2000). Constraints on mantle convection from seismic tomography. In M. A. Richards, R. Gordon, & R. D. van der Hilst (Eds.), *History and dynamics of plate motionGeophysical Monograph Series* (Vol. 121, pp. 277–288). Washington, DC: American Geophysical Union. https://doi.org/10.1029/GM121p0277

Kárason, H., & van der Hilst, R. D. (2001). Tomographic imaging of the lowermost mantle with differential times of refracted and diffracted core phases (PKP, Pdiff). *Journal of Geophysical Research*, *106*(B4), 6569–6587. https://doi.org/10.1029/2000JB900380

Karastathis, V. K., Mouzakiotis, E., Ganas, A., & Papadopoulos, G. A. (2015). High-precision relocation of seismic sequences above a dipping Moho: The case of the January-February 2014 seismic sequence on Cephalonia Island (Greece). *Solid Earth*, *6*(1), 173–184. https://doi.org/10.5194/se-6-173-2015

Kennett, B. L. N., Engdahl, E. R., & Buland, R. (1995). Constraints on seismic velocities in the Earth from travel times. *Geophysical Journal International*, *122*(1), 108–124. https://doi.org/10.1111/j.1365-246X.1995.tb03540.x

Kokinou, E., Kamberis, E., Vafidis, A., Monopolis, D., Ananiadis, G., & Zelilidis, A. (2005). Deep seismic reflection data from offshore western Greece: A new crustal model for the Ionian Sea. *Journal of Petroleum Geology*, *28*(2), 185–202. https://doi.org/10.1111/j.1747-5457.2005.tb00079.x

Kokinou, E., Papadimitriou, E., Karakostas, V., Kamberis, E., & Vallianatos, F. (2006). The Kefalonia transform zone (offshore Western Greece) with special emphasis to its prolongation towards the Ionian Abyssal Plain. *Marine Geophysical Research*, *27*(4), 241–252. https://doi.org/10.1007/s11001-006-9005-2

Konstantinou, K. I., & Melis, N. S. (2008). High-frequency shear-wave propagation across the Hellenic subduction zone. *Bulletin of the Seismological Society of America*, *98*(2), 797–803. https://doi.org/10.1785/0120060238

Koulakov, I., Kaban, M. K., Tesauro, M., & Cloetingh, S. (2009). *P*- and *S*-velocity anomalies in the upper mantle beneath Europe from tomographic inversion of ISC data. *Geophysical Journal International*, *179*(1), 345–366. https://doi.org/10.1111/j.1365-246X.2009.04279.x

Lamara, S. (2014). 3D waveform tomography of the Hellenic Subduction Zone. *PhD Thesis*, Ruhr-Universität Bochum, Germany.

Laske, G., Masters, G., Ma, Z., & Pasyanos, M. (2013). Update on CRUST1.0—A 1-degree global model of Earth's crust. *Geophysical Research Abstracts*, 15, Abstract EGU2013–2658

Li, C., van der Hilst, R. D., Engdahl, E. R., & Burdick, S. (2008). A new global model for 3-D variations of *P*-wave velocity in the Earth's mantle. *Geochemistry, Geophysics, Geosystems*, *9*, Q05018. https://doi.org/10.1029/2007GC001806

Li, X., Bock, G., Vafidis, A., Kind, R., Harjes, H. P., Hanka, W., et al. (2003). Receiver function study of the Hellenic subduction zone: Imaging crustal thickness variations and the oceanic Moho of the descending African lithosphere. *Geophysical Journal International*, *155*(2), 733–748. https://doi.org/10.1046/j.1365-246X.2003.02100.x

Ligdas, C. N., Main, I. G., & Adams, R. D. (1990). 3-D structure of the lithosphere in the Aegean region. *Geophysical Journal International*, *102*(1), 219–229. https://doi.org/10.1111/j.1365-246X.1990.tb00543.x

McClusky, S., Balassanian, S., Barka, A., Demir, C., Ergintav, S., Georgiev, I., et al. (2000). Global positioning system constraints on plate kinematics and dynamics in the eastern Mediterranean and Caucasus. *Journal of Geophysical Research*, *105*(B3), 5695–5719. https://doi.org/10.1029/1999JB900351

Meier, T., Dietrich, K., Stöckhert, B., & Harjes, H. P. (2004). One-dimensional models of shear wave velocity for the eastern Mediterranean obtained from the inversion of Rayleigh wave phase velocities and tectonic implications. *Geophysical Journal International*, *156*(1), 45–58. https://doi.org/10.1111/j.1365-246X.2004.02121.x

Meijer, P. T., & Wortel, M. J. R. (1996). Temporal variation in the stress field of the Aegean region. *Geophysical Research Letters*, *23*(5), 439–442. https://doi.org/10.1029/96GL00380

Nixon, C. W., McNeill, L. C., Bull, J. M., Bell, R. E., Gawthorpe, R. L., Henstock, T. J., et al. (2016). Rapid spatiotemporal variations in rift structure during development of the Corinth rift, Central Greece. *Tectonics*, *35*, 1225–1248. https://doi.org/10.1002/2015TC004026

Olive, J.-A., Pearce, F., Rondenay, S., & Behn, M. D. (2014). Pronounced zonation of seismic anisotropy in the Western Hellenic subduction zone and its geodynamic significance. *Earth and Planetary Science Letters*, *391*, 100–109. https://doi.org/10.1016/j.epsl.2014.01.029

Papadopoulos, G. A. (1989). Cenozoic magmatism, deep tectonics, and crustal deformation in the Aegean Sea. In C. Kissel & K. Laj (Eds.), *Paleomagnetic Rotations and Continental Deformation* (pp. 95–113). Dordrecht: Kluwer. https://doi.org/10.1007/978-94-009-0869-7_7

Papadopoulos, G. A. (1997). On the interpretation of large-scale seismic tomography images in the Aegean Sea area. *Annali di Geofisica*, *40*(1).

Papadopoulos, G. A., Karastathis, V., Kontoes, C., Charalampakis, M., Fokaefs, A., & Papoutsis, I. (2010). Crustal deformation associated with East Mediterranean strike-slip earthquakes: The 8 June 2008 Movri (NW Peloponnese), Greece, earthquake (M_w 6.4). *Tectonophysics*, *492*(1-4), 201–212. https://doi.org/10.1016/j.tecto.2010.06.012

Papanikolaou, D. J., & Royden, L. H. (2007). Disruption of the Hellenic arc: Late Miocene extensional detachment faults and steep Pliocene-Quaternary normal faults—Or what happened at Corinth? *Tectonics*, *26*, TC5003 https://doi.org/10.1029/2006TC002007

Papazachos, B. C., Karakostas, V. G., Papazachos, C. B., & Scordilis, E. M. (2000). The geometry of the Wadati-Benioff zone and lithospheric kinematics in the Hellenic arc. *Tectonophysics*, *319*(4), 275–300. https://doi.org/10.1016/S0040-1951(99)00299-1

Papazachos, B. C., & Nolet, G. (1997). *P* and *S* deep velocity structure of the Hellenic area obtained by robust nonlinear inversion of travel times. *Journal of Geophysical Research*, *102*(B4), 8349–8367. https://doi.org/10.1029/96JB03730

Pardo, M., & Suarez, G. (1995). Shape of the subducted Rivera and Cocos plates in southern Mexico: Seismic and tectonic implications. *Journal of Geophysical Research*, *100*(B7), 12357–12373. https://doi.org/10.1029/95JB00919

Pasyanos, M. E., & Walter, W. R. (2002). Crust and upper-mantle structure of North Africa, Europe, and the Middle East from inversion of surface waves. *Geophysical Journal International*, *149*(2), 463–481. https://doi.org/10.1046/j.1365-246X.2002.01663.x

Paul, A., Karabulut, H., Mutlu, A. K., & Salaün, G. (2014). A comprehensive and densely sampled map of shear-wave azimuthal anisotropy in the Aegean-Anatolia region. *Earth and Planetary Science Letters*, *389*, 14–22. https://doi.org/10.1016/j.epsl.2013.12.019

Pearce, F. D., Rondenay, S., Sachpazi, M., Charalampakis, M., & Royden, L. H. (2012). Seismic investigation of the transition from continental to oceanic subduction along the western Hellenic subduction zone. *Journal of Geophysical Research*, *117*, B07306. https://doi.org/10.1029/2011JB009023

Peng, M., Jiang, M., Li, Z.-H., Xu, Z., Zhu, L., Chan, W., et al. (2016). Complex Indian subduction style with slab fragmentation beneath the Eastern Himalayan Syntaxis revealed by teleseismic *P*-wave tomography. *Tectonophysics*, *667*, 77–86. https://doi.org/10.1016/j.tecto.2015.11.012

Pe-Piper, G., & Piper, D. J. W. (2007). Neogene backarc volcanism of the Aegean: New insights into the relationship between magmatism and tectonics. *Geological Society of America Special Papers*, *418*, 17–31.

Pérouse, E., Chamot-Rooke, N., Rabaute, A., Briole, P., Jouanne, F., Georgiev, I., & Dimitrov, D. (2012). Bridging onshore and offshore present-day kinematics of central and eastern Mediterranean: Implications for crustal dynamics and mantle flow. *Geochemistry, Geophysics, Geosystems*, *13*, Q09013. https://doi.org/10.1029/2012GC004289

Piromallo, C., & Morelli, A. (2003). *P* wave tomography of the mantle under the Alpine-Mediterranean area. *Journal of Geophysical Research*, *108*(B2), 2065. https://doi.org/10.1029/2002JB001757

Rawlinson, N., Fichtner, A., Sambridge, M., & Young, M. K. (2014). Seismic tomography and the assessment of uncertainty. *Advances in Geophysics*, *55*, 1–76. https://doi.org/10.1016/bs.agph.2014.08.001

Rawlinson, N., & Spakman, W. (2016). On the use of sensitivity tests in seismic tomography. *Geophysical Journal International*, *205*, 1211–1243.

Reilinger, R., McClusky, S., Paradissis, D., Ergintav, S., & Vernant, P. (2010). Geodetic constraints on the tectonic evolution of the Aegean region and strain accumulation along the Hellenic subduction zone. *Tectonophysics*, *488*(1-4), 22–30. https://doi.org/10.1016/j.tecto.2009.05.027

Ricou, L. E., Burg, J. P., Godfriaux, I., & Ivanov, Z. (1998). Rhodope and Vardar: The metamorphic and the olistostromic paired belts related to the Cretaceous subduction under Europe. *Geodinamica Acta*, *11*(6), 285–309. https://doi.org/10.1080/09853111.1998.11105326

Robertson, A. H. F., Dixon, J. E., Brown, S., Collins, A., Morris, A., & Pickett, et al. (1996). Alternative tectonic models for the Late Palaeozoic-Early Tertiary development of Tethys in the eastern Mediterranean region. *Geological Society of London, Special Publication*, *105*(1), 239–263. https://doi.org/10.1144/GSL.SP.1996.105.01.22

Rontogianni, S., Konstantinou, K. I., Melis, N. S., & Evangelidis, C. P. (2011). Slab stress field in the Hellenic subduction zone as inferred from intermediate-depth earthquakes. *Earth, Planets and Space*, *63*, 139–144. https://doi.org/10.5047/eps.2010.11.011

Royden, L. H., & Papanikolaou, D. J. (2011). Slab segmentation and late Cenozoic disruption of the Hellenic arc. *Geochemistry, Geophysics, Geosystems*, *12*, Q03010. https://doi.org/10.1029/2010GC003280

Sachpazi, M., Laigle, M., Charalampakis, M., Diaz, J., Kissling, E., Gesret, A., et al. (2016). Segmented Hellenic slab rollback driving Aegean deformation and seismicity. *Geophysical Research Letters*, *43*, 651–658. https://doi.org/10.1002/2015GL066818

Salaün, G., Pedersen, H. A., Paul, A., Farra, V., Karabulut, H., Hatzfeld, D., et al., & SIMBAAD Team (2012). High-resolution surface wave tomography beneath the Aegean-Anatolia region: Constraints on upper-mantle structure. *Geophysical Journal International*, *190*(1), 406–420. https://doi.org/10.1111/j.1365-246X.2012.05483.x

Schmid, C., Van der Lee, S., & Giardini, D. (2004). Delay times and shear wave splitting in the Mediterranean region. *Geophysical Journal International*, *159*(1), 275–290. https://doi.org/10.1111/j.1365-246X.2004.02381.x

Schmid, C., van der Lee, S., & Giardini, D. (2006). Correlated shear and bulk moduli to 1400 km beneath the Mediterranean region. *Physics of the Earth and Planetary Interiors*, *159*(3-4), 213–224. https://doi.org/10.1016/j.pepi.2006.07.003

Shaw, B., & Jackson, J. (2010). Earthquake mechanisms and active tectonics of the Hellenic subduction zone. *Geophysical Journal International*, *181*, 966–984.

Sodoudi, F., Brüstle, A., Meier, T., Kind, R., & Friederich, W. (2015). Receiver function images of the Hellenic subduction zone and comparison to microseismicity. *Solid Earth*, *6*(1), 135–151. https://doi.org/10.5194/se-6-135-2015

Sodoudi, F., Kind, R., Hatzfeld, D., Priestley, K., Hanka, W., Wylegalla, K., et al. (2006). Lithospheric structure of the Aegean obtained from *P* and *S* receiver functions. *Journal of Geophysical Research*, *111*, B12307. https://doi.org/10.1029/2005JB003932

Spakman, W., & Nolet, G. (1988). Imaging algorithms, accuracy and resolution in delay time tomography. In N. J. Vlaar, G. Nolet, M. J. R. Wortel, & S. A. P. L. Cloetingh (Eds.), *Mathematical geophysics: A survey of recent developments in seimology and geodynamics* (pp. 155–187). Dordrecht, Netherlands: D. Reidel.

Spakman, W., van der Lee, S., & van der Hilst, R. (1993). Travel-time tomography of the European-Mediterranean mantle down to 1400 km. *Physics of the Earth and Planetary Interiors*, *79*(1-2), 3–74. https://doi.org/10.1016/0031-9201(93)90142-V

Spakman, W., Wortel, M. J. R., & Vlaar, N. J. (1988). The Hellenic subduction zone: A tomographic image and its geodynamic implications. *Geophysical Research Letters*, *15*(1), 60–63. https://doi.org/10.1029/GL015i001p00060

Suckale, J., Rondenay, S., Sachpazi, M., Charalampakis, M., Hosa, A., & Royden, L. H. (2009). High-resolution seismic imaging of the western Hellenic subduction zone using teleseismic scattered waves. *Geophysical Journal International*, *178*(2), 775–791. https://doi.org/10.1111/j.1365-246X.2009.04170.x

Taymaz, T., Jackson, T., & McKenzie, D. (1991). Active tectonics of the north and central Aegean Sea. *Geophysical Journal International*, *106*(2), 433–490. https://doi.org/10.1111/j.1365-246X.1991.tb03906.x

Tiberi, C., Lyon-Caen, H., Hatzfeld, D., Achauer, U., Karagianni, E., Kiratzi, A., et al. (2000). Crustal and upper mantle structure beneath the Corinth rift (Greece) from a teleseismic tomography study. *Journal of Geophysical Research*, *105*(B12), 28,159–28,171. https://doi.org/10.1029/2000JB900216

van de Zedde, D. M. A., & Wortel, M. J. R. (2001). Shallow slab detachment as a transient source of heat at midlithospheric depths. *Tectonics*, *20*(6), 868–882. https://doi.org/10.1029/2001TC900018

van Hinsbergen, D. J. J., Hafkenscheid, E., Spakman, W., Meulenkamp, J. E., & Wortel, M. J. R. (2005). Nappe stacking resulting from subduction of oceanic and continental lithosphere below Greece. *Geology*, *33*(4), 325–328. https://doi.org/10.1130/G20878.1

van Keken, P. E., Hacker, B. R., Syracuse, E. M., & Abers, G. A. (2011). Subduction factory: 4. Depth-dependent flux of H_20 from subducting slabs worldwide. *Journal of Geophysical Research*, *116*, B01401. https://doi.org/10.1029/2010JB007922

Wessel, P., & Smith, W. H. (1995). New version of the generic mapping tools. *Eos, Transactions of the American Geophysical Union*, *76*(33), 329. https://doi.org/10.1029/95EO00198

Wong, S. Y. M., Ton, A., & Wortel, M. J. R. (1997). Slab detachment in continental collision zones: An analysis of controlling parameters. *Geophysical Research Letters*, *24*(16), 2095–2098. https://doi.org/10.1029/97GL01939

Wortel, M. J. R., Goes, S. D. B., & Spakman, W. (1990). Structure and seismicity of the Aegean subduction zone. *Terra Nova*, *2*(6), 554–562. https://doi.org/10.1111/j.1365-3121.1990.tb00120.x

Wortel, M. J. R., & Spakman, W. (1992). Structure and dynamics of subducted lithosphere in the Mediterranean region. *Proceedings of the Koninkliije Nederlandse Akademie van Wetenschappen*, *95*, 325–347.

Wortel, M. J. R., & Spakman, W. (2000). Subduction and slab detachment in the Mediterranean-Carpathian region. *Science*, *290*(5498), 1910–1917. https://doi.org/10.1126/science.290.5498.1910

Zhu, H., Bozdağ, E., & Tromp, J. (2015). Seismic structure of the European upper mantle based on adjoint tomography. *Geophysical Journal International*, *201*(1), 18–52. https://doi.org/10.1093/gji/ggu492